Artificial boundaries and formulations for the incompressible Navier-Stokes equations. Applications to air and blood flows.

Justine Fouchet-Incaux

Artificial boundaries and formulations for the incompressible Navier–Stokes equations. Applications to air and blood flows.

Justine Fouchet-Incaux
Laboratoire de Mathématiques d'Orsay, Université Paris-Sud 11, 91405 Orsay Cedex, France
REO project-team, INRIA Paris-Rocquencourt - BP 105 F-78153 Le Chesnay Cedex, France
justine.fouchet-incaux@inria.fr

December 26, 2013

Abstract: We deal with numerical simulations of incompressible Navier–Stokes equations in truncated domain. In this context, the formulation of these equations has to be selected carefully in order to guarantee that their associated artificial boundary conditions are relevant for the considered problem. In this paper, we review some of the formulations proposed in the literature, and their associated boundary conditions. Some numerical results linked to each formulation are also presented. We compare different schemes, giving successful computations as well as problematic ones, in order to better understand the difference between these schemes and their behaviours dealing with systems involving Neumann boundary conditions. We also review two stabilization methods which aim at suppressing the instabilities linked to these natural boundary conditions.

Key words: incompressible flow, Navier–Stokes equations, Dirichlet and Neumann boundary conditions, energy balance, *a priori* estimates, well-posedness, numerical computations, stabilization methods.

1 Introduction

The numerical simulations of incompressible Navier–Stokes equations and the choice of the boundary conditions on artificial boundaries are of great importance in many engineering fields, like biomechanics for instance (see, e.g. [75, 8, 6, 40, 38, 35]). Over the last decade, this topic has been a very active field of research and the subject of numerous works (see, e.g., [29, 1, 56, 76, 28, 55, 27, 13, 66, 43, 54, 73, 31]). The work summarized in this review is linked to the numerical simulation of the air flow in the respiratory tract. The underlying motivation is that simulations of air flows, in patient-specific geometries, may provide valuable information to physicians (e.g., in order to improve diagnosis and therapy), in the same way as done for blood flow or oncology (see e.g. [21, 14, 53, 5]).

In large (or medium size) bronchi, air is commonly modeled as a homogeneous, viscous, Newtonian and incompressible fluid (see, e.g., [1, 55, 31]). As a mathematical model, we consider therefore the system of partial differential equations involving the Navier–Stokes equations. The numerical simulation of the air flow in the respiratory system raises many questions. Among them, since the whole respiratory tree is a very complex geometry, with a lot of bifurcations, and with different scales therein, the whole domain has to be truncated and one has to choose suitable boundary conditions on the artificial boundaries.

When artificial boundaries are present, through which the fluid may enter or leave the domain, there is no general agreement on which kind of boundary conditions on these boundaries are the most appropriate on the modeling point of view. Indeed, the different boundary conditions describe the different physical phenomena, and the ability of the artificial conditions to correctly represent the real unbounded domain is crucial for the accuracy of the computed flow field in the context of an incompressible fluid. Indeed, these conditions may greatly influence the flow inside the computational domain, since any error on the flow field at the boundary may be instantaneously propagated in the whole domain.

This paper is concerned with the choice of the suitable boundary conditions and its associated formulations used to solve this problem. Indeed, whatever these conditions are, the numerical problem to be solved must be mathematically well posed. In some real-life situations, and it is the case for the lung, it is natural to prescribe a pressure on some part of the boundary. From a mathematical point of view, the pressure is only a Lagrange multiplier in the incompressible Navier–Stokes system, allowing to keep the velocity divergence free at any point. However, it is also a quantity with a physical meaning, and many papers deal with this kind of boundary conditions (see e.g. [60, 34, 3]). Unfortunately one cannot prescribe only the value of the pressure on the boundary, since such a problem is known to be ill-posed. Then the fact that boundary conditions involving pressures are often more suitable for this kind of modeling problems implies that the formulation of the Navier–Stokes equations has to be selected carefully in order to guarantee not only that their associated boundary conditions are physically relevant for this kind of modeling but also that the whole system is mathematically well-posed.

There are several formulations for the momentum equation of the Navier–Stokes system. They lead to several systems with different mathematical properties. The most elementary one is based on the basic convective form for the advection term. Using this form with natural boundary conditions, the problem can be written:

$$\begin{aligned} \rho\partial_t\mathbf{u} + \rho(\mathbf{u}\cdot\nabla)\mathbf{u} - \eta\Delta\mathbf{u} + \nabla p = 0 \text{ on } \Omega,\\ \nabla\cdot\mathbf{u} = 0 \text{ on } \Omega,\\ \mathbf{u} = 0 \text{ on } \Gamma_\ell,\\ \eta\nabla\ \mathbf{u}\cdot\mathbf{n} - p\mathbf{n} = -p_\alpha\mathbf{n}, \text{ on } \Gamma_\alpha,\ \alpha = \{\text{in},\text{out}\}. \end{aligned}$$

in the tool geometry drawn in Figure 1. Using Neumann boundary conditions implies a kinetic energy

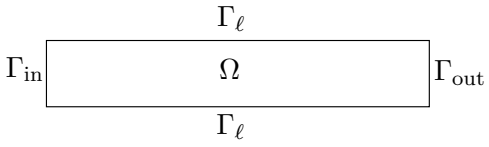

Figure 1: Basic geometry

inflow which does not allow to bound the energy. Moreover, it involves mixed boundary conditions (Dirichlet-Neumann) on each corner. Then it leads to difficulties that we will investigate in this paper. Although this basic form is often used (see, e.g., [40, 58, 74, 75, 22, 62, 31, 55, 1]), some numerical studies (see, e.g., [40, 31]) have pointed out that the stability is not guaranteed when dealing with realistic physiological or physical parameters.

In this paper, we focus on these realistic cases. In our computations, we use a tube or a bifurcation geometry which can be seen as simplified airways or a reduced artery. We also use some realistic applied pressures and physical parameters of the air (density and viscosity). We choose to deal with the air here, but we keep in mind that the blood and air behaviours are not the same since the density of the blood is one thousand times higher than the air. Finally, we are confronted with numerical difficulties which also appear in more complicated geometries.

In Section 2, we account for different formulations of the Navier–Stokes equations, in particular for the convective term, and we review some existence results for these problems. As using the basic form with natural boundary conditions implies a lack of energy conservation and then a restriction on the data, we detail an energy-preserving formulation which allows to facilitate the existence theorems, using less restrictive data. We present also the method proposed in [30], in which the velocity profile

is constrained on the artificial boundary. Then the kinetic energy flux can be controlled, and the authors obtain solutions for all time if the data are small enough.

In Section 3, we present some numerical methods to solve the different formulations seen in Section 2. We give some computations that show the effectiveness of these methods and the difference between all of them. The basic form of the convective term is usually time-discretized thanks to a semi-implicit scheme [63], which is very appealing in terms of computational cost, since it leads to a linear problem. However, as in the continuous framework, it does not allow to apply any natural boundary conditions with too high data. Indeed, in this case, instabilities develop and lead to the non-convergence of the computation. We will see in the theoretical part that the Navier–Stokes equations can be discretized using the total derivative form and the characteristics method, or using the energy-preserving form. One can also choose to apply stabilization method to overcome the problem, like the method detailed in [6, 20, 31].

2 A theoretical overview

Firstly, we are going to introduce some material in the next section.

2.1 Preliminaries

2.1.1 Basic notations

Let Ω be a bounded domain in $\mathbb{R}^d$ $(d = 2, 3)$ and let $\partial\Omega$ be its boundary. We denote by $L^2(\Omega)$ the space of real functions whose square is integrable in Ω, and by $(\cdot,\cdot)_\Omega$ and $\|\cdot\|_{L^2(\Omega)}$ the associated inner product and norm, respectively. The corresponding space of $\mathbb{R}$-valued functions $(v = (v_1, ..., v_d))$ will be denoted by boldface-type, e.g., $\mathbf{L}^2(\Omega) = (L^2(\Omega))^d$ and we will still denote by $(\cdot,\cdot)_\Omega$ and $\|\cdot\|_{L^2(\Omega)}$ the associated inner product and norm. We introduce some subspaces of $L^2(\Omega)$:

- $H^1(\Omega) = \{v \in L^2(\Omega) : \nabla v \in \mathbf{L}^2(\Omega)\}$ and $\mathbf{H}^1(\Omega) = (H^1(\Omega))^d$. We denote by $\|\cdot\|_{H^1(\Omega)}$ the two subspace norms ;
- $L^2_0(\Omega) = \{v \in L^2(\Omega) \text{ such that } \int_\Omega v = 0\}$;
- $H^1_{0,\Gamma_D}(\Omega) = \{v \in H^1(\Omega) : v = 0 \text{ on } \Gamma_{\mathrm{D}} \subset \partial\Omega\}$. $v = 0$ on Γ_{D} means that the trace of v is vanishing on Γ_{D}.

For functions depending on space and time, for a given space $\mathbf{V}$ of space dependent functions, we define (for some $T > 0$) the spaces of functions defined from the interval $[0, T]$ into $\mathbf{V}$:

$$L^p(0,T;\mathbf{V}) = \left\{\mathbf{v} : (0,T) \longrightarrow \mathbf{V} : \mathbf{v} \text{ is mesurable and } \int_0^T \|\mathbf{v}(t)\|^p_{\mathbf{V}} \mathrm{d}t < \infty\right\}$$

for $p \geq 1$, with norm $\|\mathbf{v}\|_{L^p(0,T;\mathbf{V})} = \left(\int_0^T \|\mathbf{v}(t)\|^p_{\mathbf{V}} \mathrm{d}t\right)^{1/p}$, and

$$L^\infty(0,T;\mathbf{V}) = \left\{\mathbf{v} : (0,T) \longrightarrow \mathbf{V} : \operatorname*{ess\,sup}_{t\in(0,T)} \|\mathbf{v}(t)\|_{\mathbf{V}} < \infty\right\}$$

with norm $\|\mathbf{v}\|_{L^\infty(0,T;\mathbf{V})} = \operatorname*{ess\,sup}_{t\in(0,T)} \|\mathbf{v}(t)\|_{\mathbf{V}} < \infty$. For functions which depend only on time, we define the space

$$L^\infty(0,T) = \left\{\mathbf{z} : (0,T) \longrightarrow \mathbb{R}^m : \operatorname*{ess\,sup}_{t\in(0,T)} |\mathbf{z}(t)| < \infty\right\}$$

endowed with the norm $\|\mathbf{z}\|_{L^\infty(0,T)} = \operatorname*{ess\,sup}_{t\in(0,T)} |\mathbf{z}(t)| < \infty$.

We will use bold face to indicate $\mathbb{R}^d$-valued functions as we do for function spaces. Let $\boldsymbol{\tau} = (\boldsymbol{\tau}_1, ..., \boldsymbol{\tau}_{d-1})$ be $d-1$ vectors such that $(\mathbf{n}, \boldsymbol{\tau})$ is an orthonormal basis. We denote

$$u_n = \mathbf{u}\cdot\mathbf{n} \text{ and } \mathbf{u}_{\boldsymbol{\tau}} = \mathbf{u} - u_n\mathbf{n} \text{ with } \boldsymbol{\tau} = \sum_{k=1}^{d-1} \boldsymbol{\tau}_k$$

with $\mathbf{n}$ the outward normal vector to Ω and $\mathbf{u}_{\boldsymbol{\tau}}$ the component of $\mathbf{u}$ in the tangent plane. Moreover, we simplify the notations:

$$\partial_n \mathbf{u} = \mathbf{n}\cdot\nabla\mathbf{u} = \frac{\partial \mathbf{u}}{\partial n},$$
$$\partial_{\tau_k}\mathbf{u} = \boldsymbol{\tau}_k\cdot\nabla\mathbf{u} = \frac{\partial\mathbf{u}}{\partial\tau_k},\ k = 1, ..., d-1$$
$$\text{and } \partial_{\boldsymbol{\tau}}\mathbf{u} = \sum_{k=1}^{d-1}\partial_{\tau_k}\mathbf{u}.$$

2.1.2 Tool model

For each $\mathbf{x}\in\Omega$, and at any time $t>0$, we denote by $\mathbf{u}(\mathbf{x},t) = (u_1, ..., u_d)(\mathbf{x},t)$ and $p(\mathbf{x},t)$ the fluid velocity vector field and the fluid pressure, respectively. Moreover, we consider an incompressible Newtonian fluid and we denote by ρ its density and by η its viscosity, which are both assumed to be constant. Under the previous assumptions, the motion of the fluid is described by the Navier–Stokes equations:

$$\begin{cases} \rho\partial_t\mathbf{u} + \rho(\mathbf{u}\cdot\nabla)\mathbf{u} - \nabla\cdot\boldsymbol{\sigma} = 0, \\ \nabla\cdot\mathbf{u} = 0. \end{cases} \tag{2.1}$$

where $\boldsymbol{\sigma}$ is the Cauchy tensor. Here we disregard external forces. The previous system has to be supplemented with initial conditions:

$$\mathbf{u}(\mathbf{x},0) = u_0(\mathbf{x}),\ \nabla\cdot\mathbf{u}_0(\mathbf{x}) = 0,\ \mathbf{x}\in\Omega, \tag{2.2}$$

and appropriate boundary conditions. To fix ideas, let us begin by considering a common test problem, consisting in computing non-steady flows in a rectangle (or a three-dimensional tube). The velocity is required to be zero on the upper and lower boundaries (we denote by Γ_ℓ the union of the two portions), while an upstream/downstream boundary condition is prescribed at the inlet/outlet ($\Gamma_{\text{in}}/\Gamma_{\text{out}}$). So we have $\partial\Omega = \Gamma_{\text{in}}\cup\Gamma_{\text{out}}\cup\Gamma_\ell$, with $\Gamma_{\text{in}}\cap\Gamma_{\text{out}}\cap\Gamma_\ell = \emptyset$ (see Figure 2 for the two-dimensional case). We assume that the lateral boundaries meet both Γ_{in} and Γ_{out} with an angle of $\pi/2$. Then, for now, the boundary conditions are:

$$\mathbf{u}(\mathbf{x},t) = 0,\ \mathbf{x}\in\Gamma_\ell,\ t>0, \tag{2.3}$$

supplemented with upstream and downstream boundary conditions on Γ_{in} and Γ_{out}, respectively. We will specify these conditions in the following sections. Indeed, on the flow-through parts (Γ_{in} and Γ_{out}), many types of boundary conditions can be set up to make the problem well-posed. For instance, we can impose a velocity profile at the inlet: $\mathbf{u}(\mathbf{x},t) = \mathbf{u}_D(\mathbf{x},t),\ \mathbf{x}\in\Gamma_{\text{in}},\ t>0$ on Γ_{in}. We denote by Γ_{D} the boundary where we impose a Dirichlet condition: $\Gamma_{\text{D}} = \Gamma_\ell\cup\Gamma_{\text{in}}$ if we impose a velocity profile, $\Gamma_{\text{D}} = \Gamma_\ell$ if not. Then we have $\Gamma = \partial\Omega\setminus\Gamma_{\text{D}}$.

We note that this tool geometry can be seen as simplified airways or a reduced artery. In our computations in Section 3, we use a bifurcation.

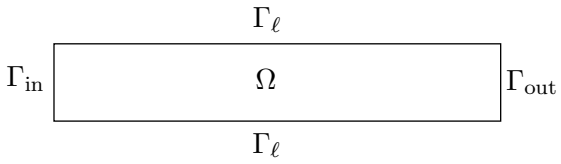

Figure 2: Basic geometry

2.1.3 Navier–Stokes equations and boundary conditions

Mathematical formulation of the tool problem. The mathematical Cauchy tensor is $\boldsymbol{\sigma} = 2\eta\mathbf{D}(\mathbf{u}) - p\mathbf{I}$, with $\mathbf{D}(\mathbf{u}) = \frac{1}{2}\left(\nabla\mathbf{u} + {}^t\nabla\mathbf{u}\right)$. Using $\nabla\cdot\mathbf{u} = 0$, we have $\nabla\cdot\boldsymbol{\sigma} = \eta\Delta\mathbf{u} - \nabla p$. Then, (2.1) reads:

$$\begin{cases} \rho\partial_t\mathbf{u} + \rho(\mathbf{u}\cdot\nabla)\mathbf{u} - \eta\Delta\mathbf{u} + \nabla p = 0, \\ \nabla\cdot\mathbf{u} = 0. \end{cases} \tag{2.4}$$

However, in this paper, we focus on artificial boundary conditions. We will see in Remark 2.1 and Section 3.2 about this stress tensor that incompressibility of the fluid allows to use a slightly different formulation, which leads to the same system (2.4) but with different boundary conditions. Indeed, always using $\nabla\cdot\mathbf{u} = 0$, we have $\nabla\cdot\boldsymbol{\sigma} = \eta\Delta\mathbf{u} - \nabla p = \nabla\cdot(\eta\nabla\mathbf{u} - p\mathbf{I})$. Here we detail the mathematical formulation of the Navier–Stokes equations using only the gradient of $\mathbf{u}$.

Both the mathematical analysis and the numerical treatment of the Navier–Stokes problem are based on weak formulations. The variational formulations of the problems will require the functional spaces:

$$\begin{aligned} &\mathbf{V} = \mathbf{H}^1_{0,\Gamma_D}(\Omega), \\ &\mathbf{V}_{\text{div}} = \{\mathbf{u}\in\mathbf{V}, \nabla\cdot\mathbf{u} = 0\} \subset \mathbf{H}^1(\Omega), \\ &\mathbf{H} = \overline{\mathbf{V}_{\text{div}}}^{\mathbf{L}^2(\Omega)} \subset \mathbf{L}^2(\Omega), \end{aligned}$$

with $\mathbf{V}$ a closed subspace of $\mathbf{H}^1(\Omega)$ such that $\mathbf{H}^1_0(\Omega) \subset \mathbf{V} \subset \mathbf{H}^1(\Omega)$, and H the compete closure of $\mathbf{V}$ for the L^2 norm. We define the following bilinear and trilinear forms (they may be redefined in the next sections):

$$\begin{aligned} a: \quad \mathbf{H}^1(\Omega)\times\mathbf{H}^1(\Omega) &\longrightarrow \mathbb{R} \\ (\mathbf{u},\mathbf{v}) &\longmapsto a(\mathbf{u},\mathbf{v}) = \eta\int_\Omega \nabla\mathbf{u} : \nabla\mathbf{v}, \\ b: \quad \mathbf{H}^1(\Omega)\times\mathbf{H}^1(\Omega)\times\mathbf{H}^1(\Omega) &\longrightarrow \mathbb{R} \\ (\mathbf{u},\mathbf{v},\mathbf{w}) &\longmapsto b(\mathbf{u},\mathbf{v},\mathbf{w}) = \rho\int_\Omega (\mathbf{u}\cdot\nabla)\mathbf{v}\cdot\mathbf{w}, \\ d: \quad \mathbf{H}^1(\Omega)\times M &\longrightarrow \mathbb{R} \\ (\mathbf{v},q) &\longmapsto d(\mathbf{v},q) = -\int_\Omega q\nabla\cdot\mathbf{v}. \end{aligned}$$

Variational formulation. The standard variational formulation of the Navier–Stokes problem (2.1)-(2.2) with the boundary condition (2.3) reads as follows:

Problem P2.1. Variational formulation without specified in/out boundary conditions
Let $\mathbf{u}_0$ belong to $\mathbf{V}_{\text{div}}$, find $\mathbf{u}$ in $L^2(0,T;\mathbf{V})$ and p in $L^2(0,T;M)$ such that for all $\mathbf{v}$ in $\mathbf{V}$, for all q

in M and for all $t \geq 0$:

$$\begin{cases} \rho\left(\partial_t \mathbf{u}, \mathbf{v}\right) + a(\mathbf{u}, \mathbf{v}) + b(\mathbf{u}, \mathbf{u}, \mathbf{v}) + \psi([\mathbf{u}, p], \mathbf{v}) + d(\mathbf{v}, p) = 0, \\ d(\mathbf{u}, q) = 0, \end{cases}$$

with $\mathbf{u}|_{t=0} = \mathbf{u}_0$,

where $\psi([\mathbf{u}, p], \mathbf{v}) = \int_\Gamma (p\mathbf{n} - \eta \nabla \mathbf{u} \cdot \mathbf{n}) \cdot \mathbf{v}$ is the boundary term coming from the integration. Next, considering free-divergence test functions $\mathbf{v}$, we obtain a second variational formulation of the problem ([70, 40]):

Problem P2.2. Variational formulation without specified in/out boundary conditions with free-divergence test functions
Let $\mathbf{u}_0$ in $\mathbf{V}_{\text{div}}$, find $\mathbf{u}$ in $L^2(0, T; \mathbf{V}_{\text{div}})$ and p in $L^2(0, T; M)$ such that for all $\mathbf{v}$ in $\mathbf{V}_{\text{div}}$, for all q in M and for all $t \geq 0$

$$\rho\left(\partial_t \mathbf{u}, \mathbf{v}\right) + a(\mathbf{u}, \mathbf{v}) + b(\mathbf{u}, \mathbf{u}, \mathbf{v}) + \psi([\mathbf{u}, p], \mathbf{v}) = 0$$

with $\mathbf{u}|_{t=0} = \mathbf{u}_0$.

The term $\psi([\mathbf{u}, p], \mathbf{v})$ will be simplified when we will choose the applied boundary conditions on Γ. In the next section, we study the energy balance without specified inflow and outflow boundary conditions. We discuss their role later.

Energy balance. Suppose that the solution of the problem exists and is regular enough. To perform an energy balance, we multiply the first equation of (2.4) by $\mathbf{u}$, we integrate over Ω and by integration by parts, we obtain:

$$\rho \int_\Omega \partial_t \mathbf{u} \cdot \mathbf{u} + \rho \int_\Omega (\mathbf{u} \cdot \nabla \mathbf{u}) \cdot \mathbf{u} + \eta \int_\Omega |\nabla \mathbf{u}|^2 + \text{ boundary terms } = 0$$

which can be written as:

$$\rho \int_\Omega \frac{1}{2} \partial_t |\mathbf{u}|^2 + \rho \int_\Omega (\mathbf{u} \cdot \nabla \mathbf{u}) \cdot \mathbf{u} + \eta \|\nabla \mathbf{u}\|^2_{L^2(\Omega)} + \text{ boundary terms } = 0.$$

Since the domain is rigid, it does not depend on time and thus

$$\int_\Omega \frac{1}{2} \partial_t |\mathbf{u}|^2 = \frac{1}{2} \frac{\mathrm{d}}{\mathrm{d}t} \int_\Omega |\mathbf{u}|^2 = \frac{1}{2} \frac{\mathrm{d}}{\mathrm{d}t} \|\mathbf{u}(\cdot, t)\|^2_{L^2(\Omega)}.$$

Moreover, we integrate by parts the convective term:

$$\begin{aligned} \int_\Omega (\mathbf{u} \cdot \nabla \mathbf{u}) \cdot \mathbf{u} &= \int_\Omega \left(\sum_i \mathbf{u}_i \partial_i \mathbf{u} \right) \cdot \mathbf{u}, \\ &= \int_\Omega \sum_j \mathbf{u}_j \sum_i \mathbf{u}_i \partial_i \mathbf{u}_j, \\ &= \frac{1}{2} \int_\Omega \sum_i \mathbf{u}_i \partial_i |\mathbf{u}|^2, \\ &= \int_\Omega \mathbf{u} \cdot \nabla \frac{|\mathbf{u}|^2}{2}, \\ &= \int_{\partial\Omega} \frac{|\mathbf{u}|^2}{2} \mathbf{u} \cdot \mathbf{n} - \int_\Omega \frac{|\mathbf{u}|^2}{2} \nabla \cdot \mathbf{u}. \end{aligned}$$

Since the velocity divergence is zero, denoting $E(t) = \frac{\rho}{2}\|\mathbf{u}(\cdot,t)\|^2_{L^2(\Omega)}$ the fluid kinetic energy, it remains:

$$\frac{\mathrm{d}}{\mathrm{d}t}E(t) = -\rho\int_{\partial\Omega}\frac{|\mathbf{u}|^2}{2}\mathbf{u}\cdot\mathbf{n} - \eta\|\nabla\mathbf{u}\|^2_{L^2(\Omega)} + \text{ boundary terms}$$

which expresses the rate of variation of kinetic energy through the power dissipated by the fluid viscosity ($\eta\|\nabla\mathbf{u}\|^2_{L^2(\Omega)}$) and the flux of kinetic energy entering (or exiting if $\mathbf{u}\cdot\mathbf{n} > 0$) the domain ($\frac{\rho}{2}\int_{\partial\Omega}|\mathbf{u}|^2\mathbf{u}\cdot\mathbf{n}$).

Until now, we have exposed the tool model and its variational formulation. Now, we have to specify the in-out boundary conditions and then simplify the term $\int_\Gamma (p\mathbf{n} - \eta\nabla\mathbf{u}\cdot\mathbf{n})\cdot\mathbf{v}$.

Essential boundary conditions. To fix ideas, we begin here with imposing a fully specified velocity:

$$\mathbf{u}(\mathbf{x},t) = 0, \text{ on } \partial\Omega.$$

Since we are imposing essential boundary conditions on all $\partial\Omega$ ($\Gamma = \emptyset$), there is no condition on the pressure but only on its gradient, so the solution p will be determined only up to an arbitrary additive constant. Then, we need to use $M = L^2_0(\Omega)$ to determine the pressure (otherwise, we can choose $M = L^2(\Omega)$). Moreover, in this case, $\Gamma_D = \partial\Omega$, and then we choose the test function to be zero on all the boundary, and the term $\int_\Gamma (p\mathbf{n} - \eta\nabla\mathbf{u}\cdot\mathbf{n})\cdot\mathbf{v}$ disappears in the variational problems. In the energy balance, it remains only:

$$\frac{\mathrm{d}}{\mathrm{d}t}E(t) = -\eta\|\nabla\mathbf{u}\|^2_{L^2(\Omega)}.$$

We note that the flux of kinetic energy is equal to zero here, which allows to get an energy balance. Time integration over an interval $(0,T)$ gives

$$E(T) = E(0) - \eta\int_0^T ||\nabla\mathbf{u}||^2_{L^2(\Omega)}.$$

The fact that the flow is viscous contribute to the dissipation of the energy. Since $E(t) = \int_\Omega \frac{\rho}{2}|\mathbf{u}(\mathbf{x},t)|^2$ is bounded over $(0,T)$, then $\mathbf{u}\in L^\infty(0,T;L^2(\Omega))$. Moreover, as the dissipated energy is bounded over $(0,T)$ ($\eta\int_0^T ||\nabla\mathbf{u}||^2_{L^2(\Omega)}$ bounded), then we have $\mathbf{u}\in L^2(0,T;H^1_{0,\partial\Omega}(\Omega))$. Thus, $\mathbf{u}\in L^\infty(0,T;L^2(\Omega))\cap L^2(0,T;H^1_{0,\partial\Omega}(\Omega))$.

The problem described by the Navier–Stokes system P2.1, in a bounded two or three dimensional domain, with prescribed velocity on the boundary $\partial\Omega = \Gamma_{\mathrm{D}}$ has weak solutions, not necessarily unique, for any Reynolds number, see e.g. [47, 70, 51]. This is based on the conservation property $(\mathbf{u}\cdot\nabla\mathbf{u},\mathbf{u}) = 0$ of the nonlinear term, which permits to have a good energy balance, as seen before.

In 2-dimensional evolutional case, the uniqueness of a weak solution on any time interval $[0,T]$ yields for the Navier–Stokes system with Dirichlet's boundary data, thanks to the control of the inertial term ([52, 51] and [70], in particular for the non-homogeneous essential boundary conditions). If the data of the problem are smooth enough, it is also a strong solution.

In 3-dimensional evolutional case, the existence of a unique strong solution is known only for sufficiently small data, e.g., $\|\nabla\mathbf{u}_0\|_{L^2(\Omega)}$ small enough (global-in-time unique solution), or on sufficiently short intervals of time, $0\le t\le T$. However, there are weak solutions on $(0,T)$, for all T, but the uniqueness of these solutions is still an open problem ([70]).

We will not deal with essential boundary conditions in this paper, except on Γ_ℓ. Indeed, we are interested in biological flows in large blood arteries or in the pulmonary airways. In these geometries,

velocity measurements are not often available, while to impose an essential boundary condition implies that a velocity profile is known. Moreover, the mechanism which governs these systems induces variations of pressure at the boundaries of the domain, in particular for the pulmonary airways since it is the diaphragm which makes us breathe. In the hemodynamic community, zero-dimensional models involving pressure are often coupled to the three-dimensional part. For more details on Dirichlet boundary conditions, we refer the reader to: [47, 44, 45, 70, 51].

Then, in the next paragraph, we deal with the prescription of pressure drops or more generally, natural boundary conditions. We are going to begin with the cases when we do not have energy conservation, and then we will review different cases when we have it.

2.2 Natural boundary conditions involving pressure drop, without energy conservation

Many practical problems in fluid dynamics are studied and conceptualized in unbounded domains. Then, these domains have to be truncated to allow the computation of the flow field in a finite computational domain. As a consequence, boundary conditions associated with these artificial boundaries are to be defined.

In this case, one can simply decide to keep the essential boundary condition at the inlet and leave the solution and the test space free at the outlet. This method is common: actually, omitting the term $\int_\Gamma (p\mathbf{n} - \eta\nabla\mathbf{u}\cdot\mathbf{n})\cdot\mathbf{v}$ in the variational formulation, we are imposing a zero-normal-stress condition at the outflow of the domain where the velocity is not known [35, 65]. This kind of boundary condition is considered in [40] and amounts to impose $p\mathbf{n} - \eta\nabla\mathbf{u}\cdot\mathbf{n} = 0$ on Γ. Then we have a homogeneous Neumann condition that occurs naturally in the variational formulation on all boundaries where no condition is imposed on the velocity. These boundary conditions are called free outflow boundary condition (see [40]) since they are commonly used as passive conditions at the artificial boundaries. The variational problems are the same that Problem P2.1 and Problem P2.2 without the boundary integral on Γ, $\psi([\mathbf{u}, p], \mathbf{v})$, since $p\mathbf{n} - \eta\nabla\mathbf{u}\cdot\mathbf{n} = 0$ on Γ.

Instead of essential boundary conditions (which suppose that the velocity profile is known), one can also decide to impose a pressure force (Neumann boundary condition) on the artificial borders which close the domain. Then we consider:

$$\eta\nabla\mathbf{u}\cdot\mathbf{n} - p\mathbf{n} = -p_\alpha\mathbf{n} \text{ on } \Gamma_\alpha,\ \alpha = \{\text{in}, \text{out}\}. \tag{2.5}$$

In all the paper, we use a constant pressure p_α on all Γ_α. This problem is called the pressure drop problem in [40].

2.2.1 Variational form

Considering (2.5), $\int_\Gamma (p\mathbf{n} - \eta\nabla\mathbf{u}\cdot\mathbf{n})\cdot\mathbf{v}$ can be replaced by the following forms on the right-hand side:

$$\begin{array}{rccl} \ell_\alpha : & \mathbf{H}^1(\Omega) & \longrightarrow & \mathbb{R} \\ & \mathbf{v} & \longmapsto & \ell_\alpha(\mathbf{v}) = -\displaystyle\int_{\Gamma_\alpha} p_\alpha\mathbf{v}\cdot\mathbf{n} \end{array}$$

with $\alpha = \{\text{in}, \text{out}\}$ and $p_\alpha \in L^2(0,T)$. If we choose $M = L^2(\Omega)$, then we can consider the variational problems:

Problem P2.3. Variational formulation of the pressure drop problem, with the basic formulation

Let $\mathbf{u}_0$ in $\mathbf{H}$, find $\mathbf{u}$ in $L^2(0,T;\mathbf{V})$ and p in $L^2(0,T;M)$ such that for all $\mathbf{v}$ in $\mathbf{V}$, for all q in M and for all $t \geq 0$

$$\begin{cases} \rho\left(\partial_t \mathbf{u}, \mathbf{v}\right) + a(\mathbf{u}, \mathbf{v}) + b(\mathbf{u}, \mathbf{u}, \mathbf{v}) + d(\mathbf{v}, p) = \ell_{\text{out}}(\mathbf{v}) + \ell_{\text{in}}(\mathbf{v}), \\ d(\mathbf{u}, q) = 0 \end{cases}$$

with $\mathbf{u}|_{t=0} = \mathbf{u}_0$.

Considering free-divergence test functions $\mathbf{v}$, we obtain a second variational formulation of the problem:

Problem P2.4. Variational formulation of the pressure drop problem, with the basic formulation, with free-divergence test functions
Let $\mathbf{u}_0$ in $\mathbf{H}$, find $\mathbf{u}$ in $L^2(0,T;\mathbf{V}_{\text{div}})$ and p in $L^2(0,T;M)$ such that for all $\mathbf{v}$ in $\mathbf{V}_{\text{div}}$, for all q in M and for all $t \geq 0$

$$\rho\left(\partial_t \mathbf{u}, \mathbf{v}\right) + a(\mathbf{u}, \mathbf{v}) + b(\mathbf{u}, \mathbf{u}, \mathbf{v}) = \ell_{\text{out}}(\mathbf{v}) + \ell_{\text{in}}(\mathbf{v})$$

with $\mathbf{u}|_{t=0} = \mathbf{u}_0$.

Despite the success of this kind of boundary conditions in modeling, there is a theoretical problem with existence and uniqueness, as explained in the next paragraph.

Remark 2.1. The choice of the viscous term formulation. In other modeling cases, in particular if one is not considering artificial boundary conditions, it could be more relevant to use the symmetric stress tensor $\boldsymbol{\sigma}$, since their associated boundary conditions allow to be more accurate in term of modeling. Since $\nabla \cdot \mathbf{u} = 0$, one has $\nabla \cdot (\nabla \mathbf{u} + {}^t\nabla \mathbf{u}) = \Delta \mathbf{u}$. Then we obtain the first equation of (2.4). Choosing $M = L^2(\Omega)$ and redefining (only here) the bilinear form:

$$\begin{array}{rccl} a: & \mathbf{H}^1(\Omega) \times \mathbf{H}^1(\Omega) & \longrightarrow & \mathbb{R} \\ & (\mathbf{u}, \mathbf{v}) & \longmapsto & a(\mathbf{u}, \mathbf{v}) = \eta \left(\left(\nabla \mathbf{u} + {}^t(\nabla \mathbf{u}) \right), \left(\nabla \mathbf{v} + {}^t(\nabla \mathbf{v}) \right) \right)_\Omega, \end{array}$$

then we can consider the variational Problem P2.4. The bilinear form a involves the symmetrized velocity gradient. Ellipticity of this bilinear form is a consequence of Korn's inequality, which ensures existence of a constant $C \geq 0$ such that

$$\int_\Omega |\nabla \mathbf{u} + {}^t\nabla \mathbf{u}|^2 \geq C \int_\Omega |\nabla \mathbf{u}|^2, \ \forall \mathbf{u} \in \mathbf{V},$$

since $|\Gamma_{\text{D}}| \neq \emptyset$. Smooth solutions of this variational pressure drop problem satisfy the boundary conditions

$$\begin{gathered} \mathbf{u} = 0 \text{ on } \Gamma_\ell, \\ \eta \left(\nabla \ \mathbf{u} + {}^t\nabla \ \mathbf{u} \right) \cdot \mathbf{n} - p\mathbf{n} = -p_\alpha \mathbf{n}, \text{ on } \Gamma_\alpha, \ \alpha = \{\text{in}, \text{out}\}. \end{gathered}$$

To use this tensor leads to physically meaningful natural boundary conditions, which properly take into account the viscous forces. They correspond to a situation in which the boundary where we impose the boundary condition is the interface between a viscous fluid (inside the domain) and a perfect fluid or an empty space. For this reason we shall call them free surface conditions.
In the situations we are interested in, the tube generally continues further, or connects onto a network of other tubes, since $\Gamma_{\text{in}}/\Gamma_{\text{out}}$ are not interfaces, but artificial boundaries. Then we choose not to use the Cauchy tensor. Then, the variational formulation leads to conditions based on the velocity gradient and natural boundary conditions become: $\eta \nabla \mathbf{u} - p\mathbf{n} = -p_\alpha \mathbf{n}$. This kind of boundary condition is

more relevant from a modeling point of view for our applications. Indeed, in the situations we are interested in, the tube generally continues further, or connects onto a network of other tubes, since they are artificial boundary conditions. We will see in Section 3.2 that these boundary conditions allow to recover the exact Poiseuille's profile, unlike the Cauchy tensor and their associated boundary conditions.
We refer to Section 3.2 for more details and to [32] for a further discussion on that matter.

2.2.2 Energy balance

Here we have:

$$\underbrace{\frac{\mathrm{d}}{\mathrm{d}t}E(t)}_{\text{Variation of kinetic energy}} = \underbrace{-\rho\int_{\Gamma_{\text{in}}\cup\Gamma_{\text{out}}}\frac{|\mathbf{u}|^2}{2}\mathbf{u}\cdot\mathbf{n}}_{\text{In/outcome of kinetic energy}} \underbrace{-\int_{\Gamma_{\text{in}}}p_{\text{in}}\mathbf{u}\cdot\mathbf{n}-\int_{\Gamma_{\text{out}}}p_{\text{out}}\mathbf{u}\cdot\mathbf{n}}_{\text{Power of } p_{\text{in}} \text{ and } p_{\text{out}}} \underbrace{-\eta\|\nabla\mathbf{u}\|^2_{L^2(\Omega)}}_{\text{Dissipation within } \Omega} \tag{2.6}$$

which expresses the rate of variation of kinetic energy through the power dissipated by the fluid viscosity ($\eta\|\nabla\mathbf{u}\|^2_{L^2(\Omega)}$) and the flux of kinetic energy entering (or exiting if $\mathbf{u}\cdot\mathbf{n}>0$) the domain ($\frac{\rho}{2}\int_{\Gamma_{\text{in}}\cup\Gamma_{\text{out}}}|\mathbf{u}|^2\mathbf{u}\cdot\mathbf{n}$). Let us first reproduce a lemma from [1], which will be useful to handle boundary integrals involving forcing pressure:

Lemma 2.1. It holds

$$\left|\int_{\Gamma_{\text{in}}}\mathbf{v}\cdot\mathbf{n}\right| \leq C\|\mathbf{v}\|_{L^2(\Omega)},\ \forall\mathbf{v}\in\mathbf{H}.$$

Using the trace inequality detailed in Lemma 2.1, Young inequality and Poincaré inequality, we can estimate the power of p_{in} and p_{out}:

$$\begin{aligned}\left|\int_{\Gamma_\alpha}p_\alpha\mathbf{u}\cdot\mathbf{n}\right| &\leq |p_\alpha|\ ||\mathbf{u}||_{L^2(\Omega)},\\ &\leq C_p|p_\alpha|\ ||\nabla\mathbf{u}||_{L^2(\Omega)},\\ &\leq \widetilde{C}|p_\alpha|^2+\frac{\eta}{4}||\nabla\mathbf{u}||^2_{L^2(\Omega)}.\end{aligned} \tag{2.7}$$

Then the dissipation of the viscous fluid can absorb the second term of (2.7), and it remains a positive term which does not disturb the energy balance.

In order to bound the energy to be able to obtain *a priori* estimates thanks to a Gronwall inequality, one has to estimate the energy that enters into the domain across the boundary where we impose natural boundary conditions, i.e. to bound the flux of kinetic energy $\frac{\rho}{2}\int_{\Gamma_{\text{in}}\cup\Gamma_{\text{out}}}|\mathbf{u}|^2\mathbf{u}\cdot\mathbf{n}$. However, for the typical situation we consider in this paper, which corresponds to the case where some fluid flows through the domain from Γ_{in} to Γ_{out}, this flux is positive at Γ_{in}, and negative at Γ_{out} but the sign of the sum is not known. This uncertainty makes it difficult to obtain *a priori* estimates, whereas they are fundamental to use the approach detailed in [48]. So, from the theoretical standpoint, the presence of free in/outlet boundary conditions drastically complicates the analysis: the existence theory is less complete than for Dirichlet boundary conditions.

2.2.3 Theory: existence and uniqueness

Finding *a priori* estimates. This problem was considered by Heywood et al. [40], where a variational approach with given mean values of the pressure across the inflow and outflow boundaries was used. The authors show that for smooth solutions, Problems P2.3 and P2.4 are equivalent, and

that these variational problems are equivalent to the basic problem (2.1)-(2.2) with the boundary conditions (2.3)-(2.5).

To obtain energy estimate and existence theorems, one has to be able to control the kinetic energy flux at the interface where energy is introduced.

In dimension 2. In dimension 2, using Sobolev injection and interpolation inequalities, we get:

$$\left|\int_\Omega (\mathbf{u}\cdot\nabla\mathbf{u})\cdot\mathbf{u}\right| \leq C\|\mathbf{u}\|_{L^2(\Omega)}\|\nabla\mathbf{u}\|^2_{L^2(\Omega)}.$$

Then one is able to bound $\mathbf{u}$, obtaining $\mathbf{u}\in L^\infty(0,T;\mathbf{H})\cap L^2(0,T;\mathbf{V}_{\rm div})$ for small data and small time. Furthermore, one can obtain existence globally in time ($T=\infty$) with additional smallness assumptions of the data.

In dimension 3. In dimension 3, the same arguments give:

$$\left|\int_\Omega (\mathbf{u}\cdot\nabla\mathbf{u})\cdot\mathbf{u}\right| \leq C\|\mathbf{u}\|^{\frac{1}{2}}_{L^2(\Omega)}\|\nabla\mathbf{u}\|^{\frac{5}{2}}_{L^2(\Omega)},$$

which is not sufficient to obtain energy estimates. It is therefore necessary either to seek other estimates or to modify the problem to obtain other estimates of the nonlinear term and prove existence results of weak or strong solutions.

In [40], the proof of a smooth solution is derived thanks to a Galerkin method based on the choice of a special basis, linked to a Stokes operator. Let us define this Stokes operator A associated with mixed Neumann-Dirichlet homogeneous boundary conditions:

Definition 2.1. For every $f\in\mathbf{H}$, there exists exactly one $\mathbf{u}\in\mathbf{V}_{\rm div}$ such that:

$$(\nabla\mathbf{u},\nabla\mathbf{v}) = (f,\mathbf{v}),\ \forall\mathbf{v}\in\mathbf{V}_{\rm div}. \tag{2.8}$$

Moreover, for each $\mathbf{u}\in\mathbf{V}_{\rm div}$, there is at most one $f\in\mathbf{H}$ satisfying (2.8). Then, (2.8) defines a bijective relation between $f\in\mathbf{H}$ and $\mathbf{u}$ in a subspace of $\mathbf{V}_{\rm div}$, denoted $\mathcal{D}(A)$. We define this set as follows:

$$\mathcal{D}(A) = \{\mathbf{u}\in\mathbf{V}_{\rm div}/\exists C>0,\ \forall\mathbf{v}\in\mathbf{V}_{\rm div},\ |(\nabla\mathbf{u},\nabla\mathbf{v})_{L^2(\Omega)}|\leq C\|\mathbf{v}\|_{L^2(\Omega)}\},$$

and we define the Stokes operator $A:\quad \mathcal{D}(A)\subset\mathbf{V}_{\rm div}\longrightarrow\mathbf{H}$ by:

$$\forall\mathbf{u}\in\mathcal{D}(A), (\nabla\mathbf{u},\nabla\mathbf{v})_\Omega = (A\mathbf{u},\mathbf{v})_\Omega,\ \forall\mathbf{v}\in\mathbf{V}_{\rm div}.$$

The operator A has the following properties:

(i) $A\in\mathcal{L}(\mathcal{D}(A),\mathbf{H})$ is invertible and its inverse is compact on $\mathbf{H}$.

(ii) A is self-adjoint.

Therefore, it admits a sequence of eigenfunctions $\{\mathbf{a}_k\}_{k\geq0}$, which is complete and orthogonal in both $\mathbf{V}_{\rm div}$ and $\mathbf{H}$. The $\{\mathbf{a}_k\}_{k\geq0}$ will be chosen as a special basis for the Galerkin approximation of the problem.

Then the main result used to prove the existence of strong solution is the following lemma from [1]:

Lemma 2.2. There exists $c_i>0$, $i=1,2$, such that, for $\mathbf{u}\in\mathcal{D}(A)$, there exits $\theta\in(0,1)$ such that

$$\|\mathbf{u}\|_{L^\infty(\Omega)}\leq c_1\|\nabla\mathbf{u}\|^\theta_{L^2(\Omega)}\|A\mathbf{u}\|^{1-\theta}_{L^2(\Omega)} \quad\text{and}\quad \|\nabla\mathbf{u}\|_{L^2(\Omega)}\leq c_2\|A\mathbf{u}\|_{L^2(\Omega)}.$$

The authors of [40] used a slightly different result of Lemma 2.2. However, their estimates rely on the assumption that $\mathbf{u}$, solution of P2.3, belongs to H^2 and this regularity is not guaranteed, see [57]. Nonetheless, except this part, their method can be used together with Lemma 2.2, which allows to prove the existence of strong solutions. Note that Lemma 2.2 relies on the fact that there exists $\epsilon > 0$ such that $\mathcal{D}(A) \subset H^{3/2+\epsilon}(\Omega)$. For this, the boundary Γ_{out} has to meet lateral boundaries Γ_ℓ at angle $\pi/2$. By taking $\mathbf{v} = A\mathbf{u}$ as a function test, they obtain $\mathbf{u} \in L^\infty(0,T;V) \cap L^2(0,T;\mathcal{D}(A))$.

To sum up. In dimensions 2 and 3, the authors of [40] proved the existence of a unique **smooth** steady solution with bounded Dirichlet norms in the case of very small data (if the prescribed mean pressure on the inflow and outflow boundaries (p_{in} and p_{out}) was properly small). We note here the additive hypothesis of regularity of the solutions.

For the unsteady problem, the authors of [40] get the existence of a smooth solution on a time interval $0 < t < T$, with $T = \infty$ if the data are sufficiently small. However, for large data, the global existence is not proven, even of a weak solution, even in two-dimension.

To conclude, it exists a unique local-in-time solution for any data, and a unique global-in-time solution for small data. Then, if the data are not small enough, we do not know what could happen in long time (see Section 3.3.1).

Remark 2.2. One can also choose to impose on $\Gamma_\alpha,\ \alpha = \{\text{in}, \text{out}\}$ the following conditions:

$$\begin{cases} \boldsymbol{\sigma} \cdot \mathbf{n} \cdot \mathbf{n} = -p_\alpha, \\ \mathbf{u} \times \mathbf{n} = 0, \end{cases}$$

and then obtain more regularity, since $\mathbf{u} \in L^2(0,T;H^2(\Omega))$, $\mathcal{D}(A) \subset H^2(\Omega)$, see [17] Section 2.4. This is better than for the pressure drop problem seen before since we only had $\mathbf{u} \in L^2(0,T;H^{3/2+\epsilon}(\Omega))$. These boundary conditions force the velocity to be normal to the outlet since a zero Dirichlet velocity is imposed for the tangential directions. See [35] for more details about this normal velocity boundary condition formulation. It has the disadvantage of directly modify the local flow fields, in particular when there are eddies which cross the boundary.

Remark 2.3. The variational Problem P2.3 and Problem P2.4 are equivalent (see [40]) to the mean pressure drop problem described in [40], which involve the following boundary conditions:

$$\left(\eta \frac{\partial u_n}{\partial n} - p\right)|_{\Gamma_\alpha} = -p_\alpha,\ \frac{\partial \mathbf{u}_\tau}{\partial n}|_{\Gamma_\alpha} = 0,\ \alpha = \{\text{in}, \text{out}\}.$$

By using Green formula, the authors see that the solution satisfies

$$\frac{1}{|\Gamma_\alpha|}\int_{\Gamma_\alpha} p = p_\alpha + \frac{\eta}{|\Gamma_\alpha|}\int_{\Gamma_\alpha} \frac{\partial u_n}{\partial n}.$$

Here, as we suppose that Γ_α is a plane section perpendicular to a cylinder pipe, the last integral vanishes and we have $\frac{1}{|\Gamma_\alpha|}\int_{\Gamma_\alpha} p = p_\alpha$. Thus, in this case, the imposed pressures p_{in} and p_{out} are the mean pressures on Γ_{in} and Γ_{out}. Then, to apply free outflow boundary condition ($p_\alpha = 0$) implies that the mean pressure on each free section is zero. Then, as indicated in [40], for a flow region with multiple outlets for instance, the flux through each outlet is highly dependent upon the relative lengths of the downstream sections, which generate a non-physical flow.

Remark 2.4. One can also prescribe the flux on this kind of boundaries: the authors of [40] introduced the prescribed flux problem, which does not have a fully equivalent formulation in terms of standard boundary conditions.

In [24], the authors consider the incompressible Navier–Stokes problem with flow rate conditions. In this paper, the authors detail an augmented formulation involving Lagrange multipliers to impose conditions on the velocity flux (in a weak sense). This kind of boundary conditions are called *defective boundary conditions*.
We refer also to [74]. In this paper, the author presents another formulation for the prescription of this kind of conditions by means of the Nitsche's method.

2.2.4 Velocity proportional to a given profile.

A way to solve the lack of energy conservation is to constrain the velocity to be proportional to a given profile. In [30], the authors can control the kinetic energy flux on the artificial boundaries.

The boundary conditions become:

$$(\Gamma_\alpha) \begin{cases} \mathbf{u} = \lambda_\alpha \mathbf{u}_\alpha, \\ \displaystyle\int_{\Gamma_\alpha} \boldsymbol{\sigma} \cdot \mathbf{n}\ \mathbf{u}_\alpha = -\int_{\Gamma_\alpha} p_\alpha \mathbf{u}_\alpha \cdot \mathbf{n}. \end{cases} \tag{2.9}$$

Then we have:

$$|\sum_\alpha \int_{\Gamma_\alpha} |\mathbf{u}|^2 (\mathbf{u}\cdot\mathbf{n})| = \sum_\alpha \gamma_\alpha \lambda_\alpha^3$$

where γ_α depends on the profile. Then the convective term can be written with a finite number of degree of freedom. The λ_α coefficients can be controlled by $||\mathbf{u}||_{L^2(\Omega)}$. Indeed, supposing that $\mathbf{u}_\alpha \cdot \mathbf{n} \neq 0$, we have:

$$|\lambda_\alpha| \leq C_\alpha ||\mathbf{u}||_{L^2(\Omega)}.$$

Then the convective term (or kinetic energy flux on $\Gamma_{\text{in}} \cup \Gamma_{\text{out}}$) can be bounded by $||\mathbf{u}||^3_{L^2(\Omega)}$, one gets *a priori* estimates (at least in small time) and one obtains energy estimates and weak solutions with a Galerkin method. Moreover, one can show that there exist solutions for all time if the data are small enough.

Numerically, such a constraint makes the system more stable i.e. there is no break-down of the iteration processes for solving the algebraic problems. Lagrange multipliers can be used to impose the velocity profile at the boundary. In [42], the authors mention that the method has little effects on the local flow, while according to [20], it can alter the flow not only near the concerned output but also in the whole domain. The computation cost is comparable to unconstrained methods ([42]). However, one has to make a modeling choice concerning the velocity profile $\mathbf{u}_\alpha$.

2.3 Natural boundary conditions involving pressure drop, with energy conservation

We have detailed in Section 2.2.4 one way to solve the lack of energy conservation, with a constraint over the velocity profile, see (2.9). One can imagine that the difficulty in the existence and uniqueness studies can be overcome also by changing the variational formulation of the problem in order to obtain energy conservation, even with natural boundary conditions. The formulation we review in this section are based on an equivalent (in the continuous field) form of the advective term. Of course, changing the variational form also changes the problem that is being solved (since the associated boundary conditions change) and may makes it unsatisfactory from a modeling point of view.

2.3.1 Total pressure

The nonlinearity in the Navier–Stokes equations can be written in several ways, which are equivalent in the continuum formulation for regular fields (since $\nabla \cdot \mathbf{u} = 0$). One leads to an energy-preserving formulations using the identity $\nabla(\frac{1}{2}|\mathbf{u}|^2) = \mathbf{u} \cdot ({}^t\nabla\mathbf{u})$. Then we can write the momentum equation of Navier–Stokes system as (see [40]):

$$\rho\partial_t\mathbf{u} + \rho(\mathbf{u}\cdot\nabla)\mathbf{u} - \rho\mathbf{u}\cdot{}^t(\nabla\mathbf{u}) - \eta\Delta\mathbf{u} = -\nabla(p + \frac{\rho}{2}|\mathbf{u}|^2) := -\nabla p_{\text{tot}}. \tag{2.10}$$

To consider the total pressure absorbs the additional term $\nabla(\frac{1}{2}|\mathbf{u}|^2)$. Then with this formulation, the natural boundary condition involves a total pressure. See [40] for more details. Choosing $M = L^2(\Omega)$ and introducing the form:

$$\begin{array}{rccl} \ell_\alpha^{\text{tot}} : & \mathbf{H}^1(\Omega) & \longrightarrow & \mathbb{R} \\ & \mathbf{v} & \longmapsto & \ell_\alpha^{\text{tot}}(\mathbf{v}) = -\displaystyle\int_{\Gamma_\alpha} p_\alpha^{\text{tot}}\mathbf{v}\cdot\mathbf{n}, \end{array}$$

we can consider the variational total drop problems:

Problem P2.5. Variational formulation of the pressure drop problem, with a form which conserves the energy
Let $\mathbf{u}_0$ in $\mathbf{H}$, find $\mathbf{u}$ in $L^2(0,T;\mathbf{V})$ and p in $L^2(0,T;M)$ such that for all $\mathbf{v}$ in $\mathbf{V}$, for all q in M and for all $t \geq 0$

$$\begin{cases} \rho\left(\partial_t\mathbf{u},\mathbf{v}\right) + a(\mathbf{u},\mathbf{v}) + b(\mathbf{u},\mathbf{u},\mathbf{v}) - \rho\displaystyle\int_\Omega \mathbf{u}\cdot(\nabla\mathbf{u})^t\mathbf{v} + d(\mathbf{v},p^{\text{tot}}) = \ell_{\text{in}}^{\text{tot}}(\mathbf{v}) + \ell_{\text{out}}^{\text{tot}}(\mathbf{v}), \\ d(\mathbf{u},q) = 0 \end{cases}$$

with $\mathbf{u}|_{t=0} = \mathbf{u}_0$.

Considering free-divergence test functions $\mathbf{v}$, we obtain a second variational formulation of the problem:

Problem P2.6. Variational formulation of the pressure drop problem, with a form which conserves the energy, with free-divergence test functions
Let $\mathbf{u}_0$ in $\mathbf{H}$, find $\mathbf{u}$ in $L^2(0,T;\mathbf{V}_{\text{div}})$ and p in $L^2(0,T;M)$ such that for all $\mathbf{v}$ in $\mathbf{V}_{\text{div}}$, for all q in M and for all $t \geq 0$

$$\rho\left(\partial_t\mathbf{u},\mathbf{v}\right) + a(\mathbf{u},\mathbf{v}) + b(\mathbf{u},\mathbf{u},\mathbf{v}) - \rho\int_\Omega \mathbf{u}\cdot(\nabla\mathbf{u})^t\mathbf{v} = \ell_{\text{in}}^{\text{tot}}(\mathbf{v}) + \ell_{\text{out}}^{\text{tot}}(\mathbf{v})$$

with $\mathbf{u}|_{t=0} = \mathbf{u}_0$.

Smooth solutions of the variational total pressure drop problem satisfy the boundary conditions

$$\mathbf{u} = 0 \text{ on } \Gamma_\ell,$$
$$\eta\nabla\ \mathbf{u}\cdot\mathbf{n} - p\mathbf{n} - \frac{\rho}{2}|\mathbf{u}|^2\mathbf{n} = -p_\alpha\mathbf{n}, \text{ on } \Gamma_\alpha,\ \alpha = \{\text{in},\text{out}\}.$$

The use of the so-called Bernoulli pressure and the additional term on the left side of (2.10) facilitate the existence theory. Indeed, in this case, the nonlinear term vanishes when one considers energy estimates, and then the flux of kinetic energy on the boundary does not appear in the energy balance (see (2.6)). In [40], the authors get smooth steady solutions for any prescriptions of steady pressures p_{in} and p_{out}. We have to pay attention to the fact that there is no guarantee of their stability if the data are large. For suitably smooth initial values and time dependent pressures $p_{\text{in}}(t)$ and $p_{\text{out}}(t)$, regardless of their size, one gets a weak solution existing for all $t \geq 0$ (i.e. a global solution). Then, we can obtain the existence of weak solutions with $\mathbf{u} \in L^\infty(0,T;\mathbf{H}) \cap L^2(0,T;\mathbf{V}_{\text{div}})$. In the case of dimension 2, $T = \infty$. In the case of dimension 3, $T = \infty$ if the data are small enough [40].

Remark 2.5. We can also consider other boundary conditions to overcome the difficulties detailed in Section 2.2. For instance, the authors of [60, 10, 11, 15, 16] directly impose the value of the dynamic pressure:

$$\mathbf{u} \times \mathbf{n} = 0,\ p + \frac{\rho}{2}|\mathbf{u}|^2 = p_\alpha \text{ on } \Gamma_\alpha,\ \alpha = \{\text{in}, \text{out}\} \tag{2.11}$$

on the artificial boundaries. Here, as we suppose that Γ_α is a plane section perpendicular to a cylinder pipe, we have $(\nabla \mathbf{u} \cdot \mathbf{n}) \cdot \mathbf{n} = 0$ and then $(\boldsymbol{\sigma}_{\text{tot}} \cdot \mathbf{n}) \cdot \mathbf{n} := ((\eta \nabla \mathbf{u}) \cdot \mathbf{n} - p - \frac{\rho}{2}|\mathbf{u}|^2) \cdot \mathbf{n} = -p - \frac{\rho}{2}|\mathbf{u}|^2$ and then the conditions (2.11) are equivalent to $\mathbf{u} \times \mathbf{n} = 0,\ (\boldsymbol{\sigma}_{\text{tot}} \cdot \mathbf{n}) \cdot \mathbf{n} = -p_\alpha$ on $\Gamma_\alpha,\ \alpha = \{\text{in}, \text{out}\}$.
In some way, these boundary conditions account for inertial effects outside the domain, see Section 4.2.2 of [55]. From a theoretical point of view, relevant *a priori* estimates can be obtained, which can be used to establish well-posedness of the problem [15, 4].
In these papers, the authors use the rotational formulation for the Navier–Stokes equations, which is another form which conserves the energy. See also [40]. We will not focus on this form in this paper.

Remark 2.6. Another way to get around the difficulties underlined in Section 2.2 is to add $\frac{\rho}{2}\mathbf{u}(\mathbf{u} \cdot \mathbf{n})$ to the constraints. In [9], the authors deal with boundary conditions on artificial boundaries of the domain, where no physical boundary data is available. They describe a new family of artificial boundary conditions, in particular (in their numerical tests)

$$\boldsymbol{\sigma}(\mathbf{u}, p) \cdot \mathbf{n} = -\frac{\rho}{2}(\mathbf{u} \cdot \mathbf{n})^-(\mathbf{u} - \mathbf{u}_{ref}) + \boldsymbol{\sigma}(\mathbf{u}_{ref}, p_{ref}) \cdot \mathbf{n}.$$

These boundary conditions lead to a well-posed problem of incompressible Navier–Stokes equations, with the global existence of a weak solution both in 2D and 3D [6]. [9] obtain that these kinds of conditions are truly robust as they can compute chaotic solutions at high Reynolds numbers, even when strong vortices cross the artificial boundary, while the standard condition produces bad effects at the outlet. We will see in Section 3.4.3 that this method has been developed in a discretized framework, see e.g. [20, 31].

2.3.2 Conclusion

Then if one uses the form which conserves the energy, existence theorems hold for less restrictive data than for the basic one. However, changing the variational form also changes the associated boundary conditions. Then the solution of the problem may be unsatisfactory from a modeling point of view. Indeed, sometimes it is more interesting to prescribe the pressure itself instead of the Bernoulli pressure (see Section 3 of [40]) and see Section 3.3.3).

3 Numerical treatment, numerical behaviour VS suitable modeling

We have seen that the nonlinearity in the Navier–Stokes equations can be written in several ways, which are equivalent in the continuum formulation (since $\nabla \cdot \mathbf{u} = 0$), but which lead to different discrete forms. Indeed, in a discrete framework, the free-divergence equation is only weakly enforced, then we do not have an exact discrete free-divergence velocity. Moreover, the divergence of the discrete velocity may grow large enough and cause significant differences between different schemes.

We will describe three forms in a discretized framework: the basic one ($\rho \partial_t \mathbf{u} + \rho(\mathbf{u} \cdot \nabla)\mathbf{u}$), the total derivatives ($\frac{\mathrm{D}\mathbf{u}}{\mathrm{D}t}$) and one which conserves the energy ($\rho \partial_t \mathbf{u} + \rho(\mathbf{u} \cdot \nabla)\mathbf{u} - \rho \mathbf{u} \cdot {}^t(\nabla \mathbf{u})$).

We will use a common test case: we solve the Navier–Stokes equations in a bifurcation, with a natural Neumann boundary condition at the inlet, and with free outlet boundary conditions at the outlet. We use $\mathbb{P}_2/\mathbb{P}_1$ approximation, $p_{\text{in}}(t) = 10\ \sin(t)$, and we run each test case during 5 seconds. Computation have been performed with the software Felisce [23], following the approach that we are going to present now.

3.1 Precisions on all the test cases shown in this section

3.1.1 Used meshes: bifurcations

In all the simulations, we use several bifurcation meshes, see Figure 3. The mother branch has a diameter equal to 0.8 cm. We note $h_{\max}$ the mesh size. In the Table 1, we give the main characteristics of the meshes used in the simulations, with the numbers of degrees of freedom if one uses a $\mathbb{P}_2/\mathbb{P}_1$ approximation.

The geometry can be seen as the beginning of the respiratory tract. Indeed, the airways can be considered as the dyadic tube network, see [77]. The blood arteries were also considered as a network, see [25].

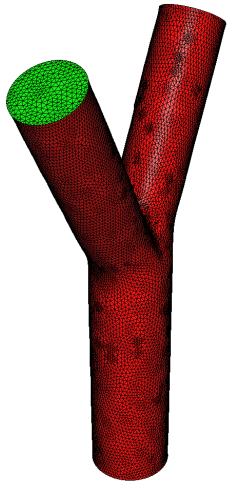

Figure 3: Bifurcation mesh

Name	Number of tetrahedra	Number of triangles (boundary elements)	Number of degree of freedom (velocity // pressure)	$h_{\max}$	Name
5M	5 354	1 286	25 494 // 1 251	0.31	coarse mesh
50M	52 034	6 946	3 1347 // 10 449	0.15	
102M	102 093	12 898	447 369 // 20 291	0.13	refined mesh
309M	308 689	29 994	1 324 017 // 58 827	0.09	

Table 1: Main characteristics of the meshes used in the simulations.

3.1.2 Used parameters and units

When one does applied mathematics and works with different communities, like doctors or physicians for instance, the considered units can change from one speaker to another. For example, the doctors used to look at centimetres of water (cmH_2O) for the pressures or litres by second (L/s) for the fluxes. Here, in all the simulations, we use the units of the international system: meters (m), kilograms (kg) and seconds (s). With these units, we express a flux in $m.s^{-1}$, and the pressure in $kg.m^{-1}.s^{-2}$ or Pascal (Pa). Moreover, we always consider air. Then we choose the density $\rho = 1,2$ $kg.m^{-3}$ and the dynamical viscosity $\eta = 2 \cdot 10^{-5}$ Pa.s.

3.1.3 Stability of the schemes and convergence of the iterative method

We will investigate two main points:

Stability of the method. A scheme is said stable when it does not amplify too much the error made at each time-step. In this paper, we show computations which lead to unstable solution, see for instance Figure 11-right.

Convergence of the iterative method. We solve the linear system with a generalized minimal residual method (GMRES). Indeed, we will see that the discretization of the Formulation A leads to a nonsymmetric matrix. In some cases, the method will be so unstable that oscillations will grow and generate a slow-down and then a break-down of the iteration processes for solving the algebraic problem. In this case, the iterative method does not converge anymore.

Table of stability. To characterize the convergence of each computation, we use the symbols:

1. ◯ : the scheme used in the computation is stable and the GMRES algorithm has converged. However the computation has not necessary reached the reference solution, due to a lack of precision. To characterize it, we use the symbols:
   (a) $\surd$: the flux at the inlet/outlets has a good agreement with the flux of the reference solution.
   (b) $\times$: the flux at the inlet/outlets has a poor agreement with the flux of the reference solution.
2. ⊠ : the GMRES algorithm converges at each time-step but the scheme used in the computation is not stable: some errors grow and lead to a nonphysical solution.
3. ■ : convergence failed in linear solver because the maximum number of iterations is reached. Then the linear system cannot be solved and the computation stops before the final time.

For each method, we define the reference solution as the solution computed with a mesh fine enough and a time-step small enough in order to obtain converged fluxes at the inlet/outlets.

Precisions on the GMRES algorithm. A restarted GMRES algorithm is used to solve the linear systems. The method is restarted after 200 iterations. We use a relative tolerance of 10^{-6} and an absolute one of 10^{-8}. The maximum number of iterations is 10 000 and the solver is initialized with the previous solution.

3.1.4 Finite element discretization

In this paper, we focus on a mixed formulation of the Navier–Stokes equations. We refer to [12, 36, 69] for an overview of projection methods.

Let $\mathcal{T}_h$ be a family of quasi-uniform triangulations $\mathcal{T}_h = \{K\}$ of Ω with mesh size h. For a given positive integer r, we introduce the finite element space

$$\mathbf{V}_h = \{\mathbf{v} \in \mathbf{V} : \ \mathbf{v}|_K \in P_r(K) \ \forall K \in \mathcal{T}_h\} \subset \mathbf{V} = \mathbf{H}^1_{0,\Gamma_D}(\Omega)$$

which is the space of continuous piecewise polynomial functions of degree r, and then an approximation of $\mathbf{V}$. Let $\mathbf{u}_h \in \mathbf{V}_h$ be the discretized-in-space function.

3.2 Diffusion term: comparison between symmetric and nonsymmetric stress tensor

We have seen in Remark 2.1 that the two forms are equivalent in a continuous framework if $\nabla \cdot \mathbf{u} = 0$ since $\nabla \cdot ({}^t\nabla \mathbf{u}) = \nabla(\nabla \cdot \mathbf{u})$ and $\nabla \cdot (\nabla \mathbf{u}) = \Delta \mathbf{u}$. Then with this in hand, we have:

$$-2\eta \nabla \cdot \left(\frac{\nabla \mathbf{u} + {}^t\nabla \mathbf{u}}{2} \right) = -\eta \Delta \mathbf{u}.$$

The discussion on these forms started in the late 90s (see Heywood and coworkers [40]) and it is still active (see [50]).

3.2.1 Numerical point of view

Whereas the matrix corresponding to the use of nonsymmetric tensor is block-diagonal (scalar Laplace operator for each component of the velocity), it is no longer block-diagonal using the symmetrized tensor. Then the nonsymmetrized stress tensor is usually simplest for computations.

Moreover, the two formulations with the two tensors are equivalent in a continuous framework since $\nabla \cdot \mathbf{u} = 0$ but not at the discrete level. Let $\mathbf{u}_h$ represents the numerical finite element solution. In a numerical simulation, $\nabla \cdot \mathbf{u}_h$ is not exactly equal to 0, then the difference may be significant. In particular, the differences were stronger when one uses a coarse mesh, since the derivative computations are less accurate. In most of the applications we cannot use the necessary mesh resolution and then we are doing a mistake considering the nonsymmetric one.

In [39], the authors show that differences are very small but still there (they compared numerically the two forms with benchmarks). They also mention that the difference is stronger for the flows that contain more rotational structures, then the difference in computational results should be more pronounced in turbulent flows where Reynolds number is very high.

3.2.2 Physical point of view

In two dimensions and with a planar boundary, the surface traction vector can be expressed as:

$$\begin{aligned}
\boldsymbol{\sigma} \cdot \mathbf{n} &= \eta(\nabla \mathbf{u} + {}^t\nabla \mathbf{u}) \cdot \mathbf{n} - p\mathbf{n}, \\
&= \eta(\frac{\partial \mathbf{u}}{\partial n} + \nabla(\mathbf{n} \cdot \mathbf{u})) - p\mathbf{n}, \\
&= \eta(\frac{\partial \mathbf{u}}{\partial n} + \nabla u_n) - p\mathbf{n}, \\
&= \left(2\eta \frac{\partial u_n}{\partial n} - p \right) \mathbf{n} + \eta \left(\frac{\partial u_n}{\partial \tau} + \frac{\partial \mathbf{u}_\tau}{\partial n} \right) \boldsymbol{\tau}.
\end{aligned}$$

If we note $\mathbf{F} = \boldsymbol{\sigma} \cdot \mathbf{n}$, we have $\mathbf{F} = F_\mathbf{n}\mathbf{n} + F_{\boldsymbol{\tau}}\boldsymbol{\tau}$, with $F_\mathbf{n} = 2\eta \frac{\partial u_n}{\partial n} - p$ and $F_{\boldsymbol{\tau}} = \eta \left(\frac{\partial u_n}{\partial \tau} + \frac{\partial \mathbf{u}_\tau}{\partial n} \right)$ the normal and tangential (shear) components of $\mathbf{F}$. Then $F_\mathbf{n}\mathbf{n}$ and $F_\tau \boldsymbol{\tau}$ are supplied by the physics of the problem we are modeling.

Remark 3.1. Note that it is not necessary to impose $F_\mathbf{n}$ and F_τ simultaneously on the boundary. One can enforce $F_{\boldsymbol{\tau}}$ and $\mathbf{u} \cdot \mathbf{n}$ or $F_\mathbf{n}$ and $\mathbf{u} \cdot \boldsymbol{\tau}_k$, $k = 1, ..., d-1$. For instance, we can consider perfect boundary conditions, solving the Navier–Stokes equations with a condition of no tangential friction (i.e. perfect slip) and with a nonpenetration condition on the velocity: $\boldsymbol{\tau} \cdot \left(\eta \left(\nabla \mathbf{u} + {}^t\nabla \mathbf{u} \right) \cdot \mathbf{n} - p\mathbf{n} \right) = 0 \quad ; \quad \mathbf{u} \cdot \mathbf{n} = 0$. However, this case does not correspond to our modeling framework. See [61] for more details.

With the unsymmetrized tensor, we have:

$$\begin{aligned}\eta\nabla\mathbf{u}\cdot\mathbf{n}-p\mathbf{n} &= \eta\frac{\partial\mathbf{u}}{\partial n}-p\mathbf{n},\\ &= \left(\eta\frac{\partial u_n}{\partial n}-p\right)\mathbf{n}+\eta\frac{\partial\mathbf{u}_\tau}{\partial n}\boldsymbol{\tau}.\end{aligned}$$

Here we have $F_{\mathbf{n}} = \eta\frac{\partial u_n}{\partial n} - p$ and $F_{\boldsymbol{\tau}} = \eta\frac{\partial \mathbf{u}_\tau}{\partial n}$. The natural boundary conditions with the weak formulation based on the unsymmetrized tensor often perform better than the same results using the symmetric form since they allow to recover the exact Poiseuille's profile. This is related to the fact that $\frac{\partial\mathbf{u}_\tau}{\partial n}$ is often a better outflow boundary condition than $\frac{\partial u_n}{\partial\tau}+\frac{\partial\mathbf{u}_\tau}{\partial n}=0$, which is actually an interface condition as seen in Remark 2.1.

Indeed, [46] demonstrated how the condition $\frac{\partial u_n}{\partial\tau}+\frac{\partial\mathbf{u}_\tau}{\partial n}=0$ can "destroy" a simulation of a Stokes flow (with a Poiseuille profile) in a channel near the outflow. Indeed, the boundary condition $\mathbf{u}=0$ at the top and bottom walls and $\mathbf{u}\neq 0$ (in particular $\mathbf{u}_n\neq 0$) at the outlet imply that $\frac{\partial u_n}{\partial\tau}\neq 0$ and then that $\frac{\partial\mathbf{u}_\tau}{\partial n}\neq 0$. Thus, a two-dimensional flow is generated when a unidirectional flow is desired. Moreover, for high Reynolds numbers, the term $2\eta\frac{\partial u_n}{\partial n}$ tends to be small compared with p. Then the factor of 1 or 2 is not important in many cases.

Then if we simulate a flow in a channel using successively standard and symmetric tensors at the outlet as made in [46] and in [40], we observe that if one uses the symmetric one, the behaviour of the fluid at the outlet of the domain does not match with an artificial truncation (see Figure 4). Indeed, the velocity vectors go outward, like at the end of a pipe. For this modeling case, we need the natural boundary conditions induced by the use of the nonsymmetric tensor, which is then better in this case. We refer the reader to [33] for a further discussion on that matter.

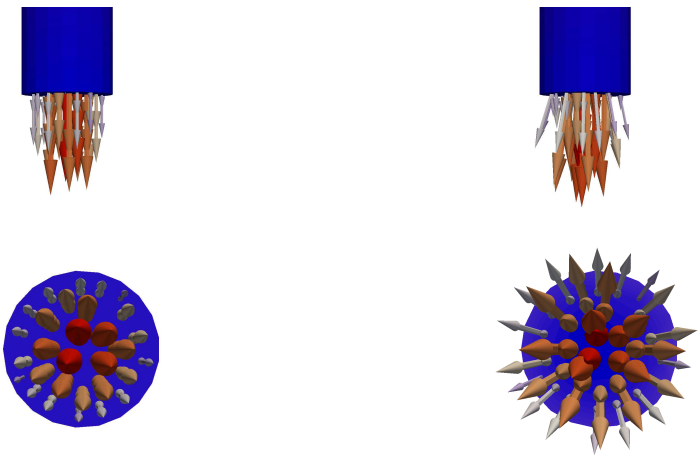

Figure 4: Outflow with nonsymmetric (left) and symmetric (right) tensor.

To conclude, even if one has to keep in mind that the physical meaningful viscous form is the symmetric one, the nonsymmetric form is the more suitable when modeling flows through a truncated domain.

Remark 3.2. In a fluid-structure interaction framework, it is necessary to choose the symmetric tensor. Indeed, it directly give the right natural boundary condition for the structure problem.

3.2.3 Conclusion

Here, we only presented two forms for the viscous term. For an exhaustive overview of the different possibilities, the reader is referred to the review papers by [32] and [65]. To sum up, we can use a lots of forms for this terms, which lead to different natural boundary conditions. We have to pay attention to the fact that these conditions are satisfactory from a modeling point of view. In our case, the behaviour of the outflow boundary condition using the nonsymmetric form, with the simplicity and lower cost, makes the use of the conventional weak form advantageous in our modeling cases.

The choice of the formulation for the diffusive term does not change the problem linked to the lack of energy conservation seen in Section 2.2. In the next section, we come back to this topic.

3.3 Finite element discretization of the convective term

The nonlinearity in the Navier–Stokes equations can be written in several ways, which are equivalent in the continuum formulation of the Navier–Stokes equations (since $\nabla \cdot \mathbf{u} = 0$), but which lead to different discrete formulations with different algorithmic costs, conserved quantities, and approximation accuracy ([32, 37]).

3.3.1 Basic formulation of the convective form. (Formulation A, see Section 2.2.1)

We saw there were two different ways to write the variational problem (considering or not free-divergence test functions, see problems P2.3 and P2.4). Then there are two different numerical approaches:

- At first, we choose a finite dimensional subspace of the divergence free subspace $\mathbf{V}_{\text{div}}$, denoting it $\mathbf{V}_{\text{div},h} = \{\mathbf{v}_h \in \mathbf{V}_h : \ (\nabla \cdot \mathbf{v}_h, q_h) = 0 \ \forall q_h \in M_h\}$. Then we have the discrete problem: for each $t \in [0,T]$, seek $\mathbf{u}_h(t,\cdot) \in \mathbf{V}_{\text{div},h}$ such that:

$$\begin{cases} \rho\left(\dfrac{\mathrm{d}}{\mathrm{d}t}\left(\mathbf{u}_h(t),\mathbf{v}_h\right) + b(\mathbf{u}_h(t),\mathbf{u}_h(t),\mathbf{v}_h)\right) \\ \qquad +a(\mathbf{u}_h(t),\mathbf{v}_h) = \ell_{\text{in}}(\mathbf{v}_h) + \ell_{\text{out}}(\mathbf{v}_h) \quad \forall \mathbf{v}_h \in \mathbf{V}_{\text{div},h}, \ t \in (0,T), \\ \mathbf{u}_h(0) = \mathbf{u}_{0,h}, \end{cases}$$

  where $\mathbf{u}_{0,h} \in \mathbf{V}_{\text{div},h}$ is an approximation to the initial data $\mathbf{u}_0$. This is therefore a Galerkin approximation to Problem P2.4.

- Now, to approximate the Problem P2.3, one has to consider the subspace M_h which is an approximation of M. Then the approximated problem becomes: for each $t \in [0,T]$, seek $\mathbf{u}_h(\cdot,t) \in \mathbf{V}_h$ and $p_h(\cdot,t) \in M_h$ such that:

$$\begin{cases} \rho\left(\dfrac{\mathrm{d}}{\mathrm{d}t}\left(\mathbf{u}_h(t),\mathbf{v}_h\right) + b(\mathbf{u}_h(t),\mathbf{u}_h(t),\mathbf{v}_h)\right) & \\ \qquad +a(\mathbf{u}_h(t),\mathbf{v}_h) + d(\mathbf{v}_h,p_h(t)) = \ell_{\text{in}}(\mathbf{v}_h) + \ell_{\text{out}}(\mathbf{v}_h), & \forall \mathbf{v}_h \in \mathbf{V}_h, \ t \in (0,T), \\ d(\mathbf{u}_h(t),q_h) = 0, & \forall q_h \in M_h, \ t \in (0,T), \\ \mathbf{u}_h(0) = \mathbf{u}_{0,h}, & \mathbf{u}_{0,h} \in \mathbf{V}_h. \end{cases}$$

Let $\Delta t > 0$ be the time-step and $t^n = n\Delta t$, $n \in \mathbb{N}$ the discrete time. We denote by $\mathbf{u}^n$ the approximation solution at time t^n. In what follows, let us take the simplest scheme in time: the backward Euler scheme.

The solver uses a $\mathbb{P}_2$ space for the velocity and a $\mathbb{P}_1$ space for the pressure, so that the inf-sup condition is satisfied ([7]). The linear systems obtained are then solved using a GMRES iterative method, preconditioned by a ILU method.

Implicit treatment. We can treat the convective term with an Euler implicit scheme [61]:

$$\frac{\rho}{\Delta t}\left(\mathbf{u}_h^{n+1}, \mathbf{v}_h\right)_\Omega + \eta\left(\nabla \mathbf{u}_h^{n+1}, \nabla \mathbf{v}_h\right)_\Omega + \rho\left(\mathbf{u}_h^{n+1} \cdot \nabla \mathbf{u}_h^{n+1}, \mathbf{v}_h\right)_\Omega = \ell_{\text{in}}(\mathbf{v}_h) + \ell_{\text{out}}(\mathbf{v}_h) + \frac{\rho}{\Delta t}\left(\mathbf{u}_h^{n}, \mathbf{v}_h\right)_\Omega .$$

With this scheme, we must solve a nonlinear system at each time-step.

Semi-implicit treatment. A semi-implicit discretization leads:

$$\frac{\rho}{\Delta t}\left(\mathbf{u}_h^{n+1}, \mathbf{v}_h\right)_\Omega + \eta\left(\nabla \mathbf{u}_h^{n+1}, \nabla \mathbf{v}_h\right)_\Omega + \rho\left(\mathbf{u}_h^{n} \cdot \nabla \mathbf{u}_h^{n+1}, \mathbf{v}_h\right)_\Omega = \ell_{\text{in}}(\mathbf{v}_h) + \ell_{\text{out}}(\mathbf{v}_h) + \frac{\rho}{\Delta t}\left(\mathbf{u}_h^{n}, \mathbf{v}_h\right)_\Omega .$$

This scheme is simple and almost fully implicit. However, at each iteration, one needs to assemble a matrix and to solve a nonsymmetric linear system. We are going to use it in the next simulations.

If one considers only the semi-discretized-in-time system:

$$\begin{aligned} \rho\frac{\mathbf{u}^{n+1}(\mathbf{x}) - \mathbf{u}^{n}(\mathbf{x})}{\Delta t} + \rho\mathbf{u}^n \cdot \nabla \mathbf{u}^{n+1} - \eta\Delta \mathbf{u}^{n+1} + \nabla p &= f, \\ \nabla \cdot \mathbf{u}^{n+1} &= 0, \end{aligned} \tag{3.1}$$

with homogeneous Dirichlet boundary conditions, we note that the scheme satisfies a energy estimate which ensures its stability. Indeed, for a family of fields $(\mathbf{u}^n)_n \in \mathbf{H}^1_{\text{div}}(\Omega)$, if we define $c(\mathbf{w}, \mathbf{z}, \mathbf{v}) = \int_\Omega [(\mathbf{w} \cdot \nabla)\mathbf{z}] \cdot \mathbf{v}$, we have $c(\mathbf{u}^n, \mathbf{u}^{n+1}, \mathbf{u}^{n+1}) = 0$. Then if we multiply the equation (3.1) by $\mathbf{u}^{n+1}$, integrating over Ω, we get for all n :

$$\rho\frac{1}{2}\frac{1}{\Delta t}\|\mathbf{u}^{n+1}\|^2_{L^2(\Omega)} + \frac{1}{2}\eta\|\nabla \mathbf{u}^{n+1}\|^2_{L^2(\Omega)} \leq \rho\frac{1}{2}\frac{1}{\Delta t}\|\mathbf{u}^{n}\|^2_{L^2(\Omega)} + \frac{C_p}{2\eta}\|f^n\|^2_{L^2(\Omega)}$$

where C_p is the constant from the Poincaré inequality. If we sum from $n = 0$ to $n = N-1$, we obtain:

$$\rho\|\mathbf{u}^N\|^2_{L^2(\Omega)} + \eta\Delta t\sum_{k=1}^{N}\|\nabla \mathbf{u}^k\|^2_{L^2(\Omega)} \leq \rho\|\mathbf{u}^0\|^2_{L^2(\Omega)} + \frac{TC_p}{\eta}\sum_{n=0}^{N-1}\|f\|^2_{L^2(\Omega)}.$$

Then the scheme allows to bound the L^2 norm. However, when we discretize it in space, we do not have $\nabla \cdot \mathbf{u}_h = 0$ anymore. Then $c(\mathbf{u}^n, \mathbf{u}^{n+1}, \mathbf{u}^{n+1}) = 0$ does no longer hold, and we lose the L^2-norm bound. Then it is not unconditionally stable. As a consequence, this scheme is usually used for moderate Reynolds number, see [61]. We will develop later some stabilizing solutions, see Section 3.4.

In Section 2.2, we have seen that for large applied pressures, the global existence of a weak solution is not proven. Indeed, it seems that the existence theorem may be valid only for very small data. However, the authors of [40] explain that one may have difficulties to compute the solution of systems involving high applied pressures but that these difficulties have not actually arisen in their computations. In Section 3.3.4, we will highlight them, showing different test-cases which lead to the non-convergence of the scheme.

Test case: $\Delta t = 0.01$, nonsymmetric tensor, $p_{\text{in}}(t) = 10\sin(t)$

On Figure 5, we observe the beginning of an instability, which lead to the blow up of the solution at the inlet, in particular the velocity vector field. The instability is developing at the inlet, where we are imposing a Neumann boundary condition.

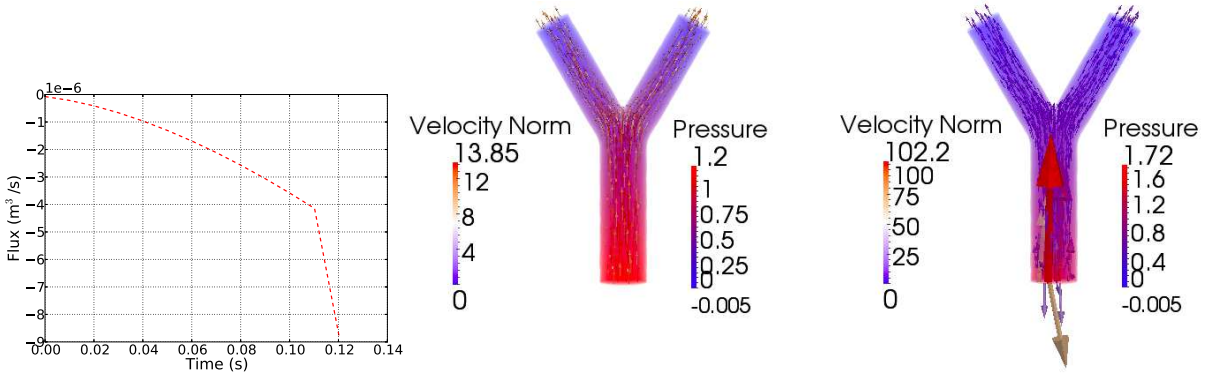

Figure 5: Left: flux (m^3/s) as a function of time (s) at the inlet. Center and right: velocity vector and pressure fields at $t = 0.12$ (center) and at $t = 0.13$ (right). Nonsymmetric stress tensor, basic formulation of the convective term, coarse mesh, $\Delta t = 0.01$ and $p_{\text{in}}(t) = 10\sin(t)$. Velocity norm in 10^{-6} m^3/s and pressure in 10^{-1} Pa.

Test case: $\Delta t = 0.01$, symmetric tensor, $p_{\text{in}}(t) = 10\sin(t)$

The same instability is developing when one uses the symmetric tensor, see Figure 6.

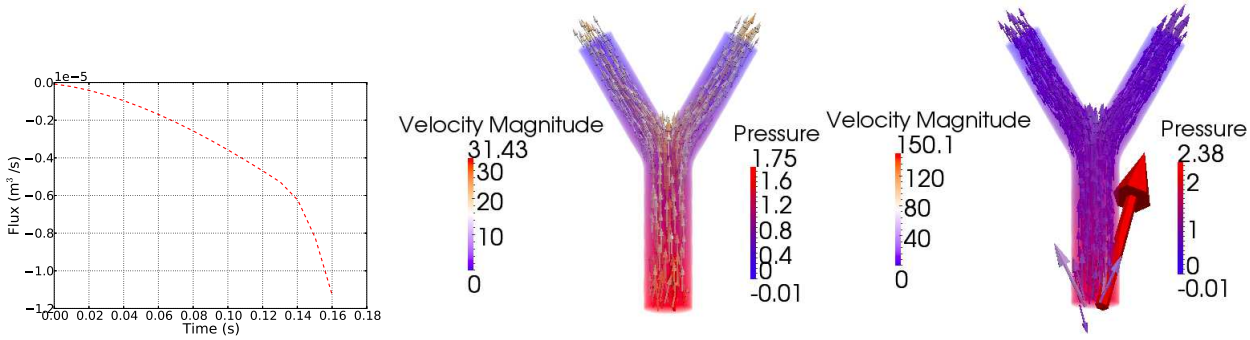

Figure 6: Left: flux (m^3/s) as a function of time (s) at the inlet. Center and right: velocity vector and pressure fields at $t = 0.17$ (center) and at $t = 0.183$ (right). Symmetric stress tensor, basic formulation of the convective term, coarse mesh, $\Delta t = 0.01$ and $p_{\text{in}}(t) = 10\sin(t)$. Velocity magnitude in 10^{-6} m^3/s and pressure in 10^{-1} Pa.

Test case: $\Delta t = 0.001$, symmetric tensor, $p_{\text{in}}(t) = 10\sin(t)$

It is still developing when one uses a lower time-step, see Figure 7.

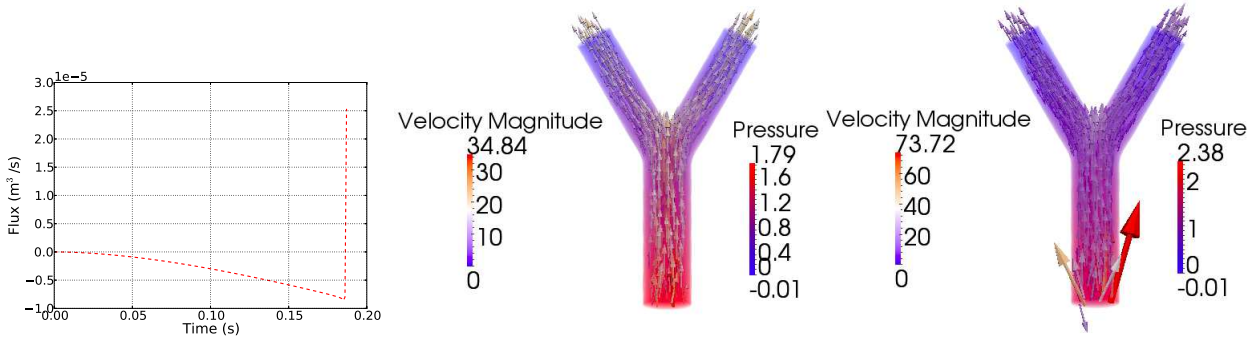

Figure 7: Left: flux (m^3/s) as a function of time (s) at the inlet. Center and right: velocity vector and pressure fields at $t = 0.17$ (center) and at $t = 0.183$ (right). Symmetric stress tensor, basic formulation of the convective term, coarse mesh, $\Delta t = 0.001$ and $p_{\text{in}}(t) = 10\sin(t)$. Velocity magnitude in 10^{-6} m^3/s and pressure in 10^{-1} Pa.

3.3.2 Total derivatives: characteristics method. (Formulation B)

We can express the terms $\partial_t \mathbf{u} + (\mathbf{u}\cdot\nabla)\cdot\mathbf{u}$ in an alternative form: the total derivative $\frac{\mathrm{D}\mathbf{u}}{\mathrm{D}t}$. We refer to [59, 2]. Let $x \in \Omega$ and $t \in [0,T]$. We define the characteristic $\mathbf{X} = \mathbf{X}(\tau;t,\mathbf{x})$ associated with the velocity field $\mathbf{u}$, such that

$$\begin{cases} \dfrac{\mathrm{d}\mathbf{X}(\tau;t,\mathbf{x})}{\mathrm{d}\tau} = \mathbf{u}(\mathbf{X}(\tau;t,\mathbf{x}),\tau), \ \tau \in (0,T), \\ \mathbf{X}(t;t,\mathbf{x}) = \mathbf{x}. \end{cases} \tag{3.2}$$

$\mathbf{X}(\tau;t,\mathbf{x})$ is the position at time τ of the particle which is in $\mathbf{x}$ at time t. With these characteristics, we can display the total derivative in the momentum equation of the Navier–Stokes system and then absorb the convective nonlinearity. We have

$$\frac{\mathrm{d}}{\mathrm{d}\tau}[\mathbf{u}(\mathbf{X}(\tau;t,\mathbf{x}),\tau)] = \left(\frac{\mathrm{d}\mathbf{X}}{\mathrm{d}\tau}(\tau;t,\mathbf{x})\cdot\nabla\right)\mathbf{u}(\mathbf{X}(\tau;t,\mathbf{x}),\tau)] + \frac{\partial\mathbf{u}}{\partial\tau}(\mathbf{X}(\tau;t,\mathbf{x}),\tau).$$

Then we get, with (3.2):

$$\frac{\mathrm{d}}{\mathrm{d}\tau}[\mathbf{u}(\mathbf{X}(\tau;t,\mathbf{x}),\tau)]|_{\tau=t} = (\mathbf{u}\cdot\nabla)\mathbf{u}(\mathbf{x},t) + \frac{\partial\mathbf{u}}{\partial\tau}(\mathbf{x},t)$$

and the momentum equation can be written with Lagrangian form:

$$\frac{\mathrm{d}}{\mathrm{d}t}[\mathbf{u}(\mathbf{X}(\tau;t,\mathbf{x}),\tau)]|_{\tau=t} - \eta\Delta\mathbf{u} + \nabla p = 0$$

with $(\mathbf{x},t) \in \Omega\times(0,T)$. In a discretized framework, the problem becomes:

$$\begin{aligned} &\text{Find}(\mathbf{u}_h^{k+1}, p_h^{k+1}) \in \mathbf{V}_h \times M_h \text{ such that} \\ &\left(\frac{\mathbf{u}_h^{k+1} - \mathbf{u}_h^k \circ \mathbf{X}_h^k}{\Delta t}, \mathbf{v}_h\right) + a(\mathbf{u}_h^{k+1}, \mathbf{v}_h) = \ell_{\text{in}}(\mathbf{v}_h) + \ell_{\text{out}}(\mathbf{v}_h), \quad \forall \mathbf{v}_h \in \mathbf{V}_h, \end{aligned}$$

where $\mathbf{u}_h^k \circ \mathbf{X}_h^k = \mathbf{u}_h^k(\mathbf{X}_h^k,\cdot)$.

Here, $\mathbf{X}_h^k(\mathbf{x})$ is an approximation of the foot of the characteristic at time t^k which passes through $\mathbf{x}$ at time t^{k+1} under the action of $\mathbf{u}^k$. More precisely, $\mathbf{X}_h^k(\mathbf{x}) = \phi(t^k;t^{k+1},\mathbf{x})$ where $\phi = \phi(\cdot,t^{k+1},\mathbf{x})$

satisfies

$$\frac{\mathrm{d}\phi}{\mathrm{d}t}(t;t^{k+1},\mathbf{x}) = \mathbf{u}_h^k(\phi(t;t^{k+1},\mathbf{x})),\ t^k \le t < t^{k+1},$$
$$\phi(t^{k+1};t^{k+1},\mathbf{x}) = \mathbf{x}. \tag{3.3}$$

If one uses an Euler scheme, it holds $\mathbf{X}_h^k(\mathbf{x}) \simeq \mathbf{x} - \Delta t\ \mathbf{u}_h^k$. Actually, in a time-discretized framework, we do not solve (3.3) with the global time-step Δt but we use a smaller time-step $\Delta t_{\text{charact}}$, adapted to the used scheme.

We note that the linear system obtained is symmetric and the matrix is independent of k. If $\mathbf{X}_h^k$ is well chosen, this scheme is unconditionally stable for all η and Δt [59], even if it does not conserve the energy (see [67]). Then one of the most interesting advantages of this method is that it permits to use large global time-steps since it does not involve any restrictive stability condition on Δt. However, according to the scheme which is used to solve the system (3.3), a constraint on the time-step $\Delta t_{\text{charact}}$ (the so-called CFL, Courant-Friedrichs-Levy) may be necessary.

The method is accurate and stable but rather costly because one has to backtrack the characteristic lines for each vertex. Then a parallel computation raises difficulties, in particular with the high number of needed communications between processors.

Remark 3.3. On the treatment of the boundaries
If the considered characteristic line is going outside the domain when one is backtracking it, a standard procedure is to choose $\widetilde{\mathbf{X}}_h^k(\mathbf{x}) = \mathbf{X}_h^k(\mathbf{x}) = \phi(\widetilde{t}^k;t^{k+1},\mathbf{x})$ instead of $\mathbf{X}_h^k(\mathbf{x}) = \phi(t^k;t^{k+1},\mathbf{x})$, with $\widetilde{t}^k$ the time at which the particle, which is in $\mathbf{x}$ at time t^{k+1}, meets the inlet. Then $\mathbf{X}_h^k(\mathbf{x})$ is on the boundary of the domain, and not outside. The fact that this boundary treatment may have a stabilization effect is not excluded.

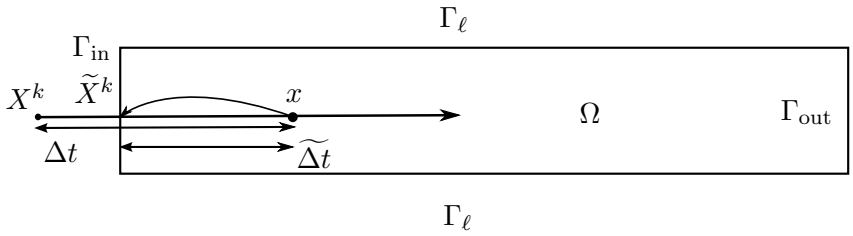

Figure 8: Boundary treatment with the characteristics method.

Test case: On Figure 9, we have the same time-step that in Figures 5-6-7. Here we are not using a scheme based on a central-differences-like discretization of the convective term. And we observe that there is no instability. In Figure 10, we observe that the scheme allows to capture well the vortices in the reversal flow.

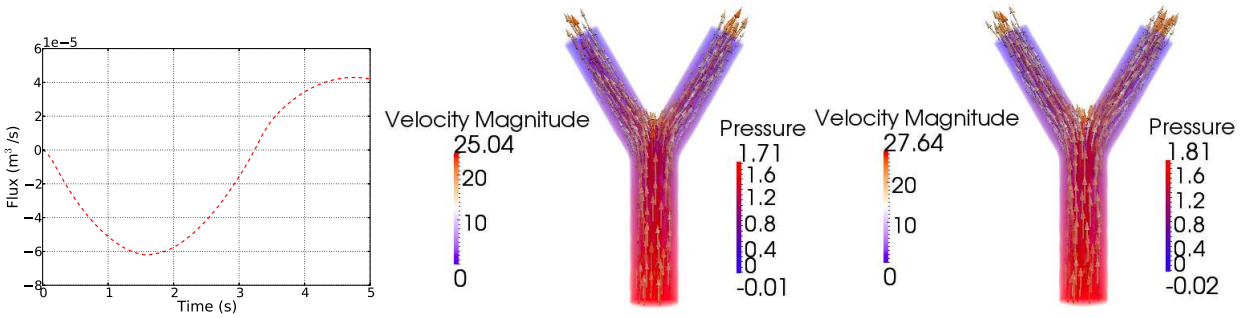

Figure 9: Left: flux (m^3/s) as a function of time (s) at the inlet. Center and right: velocity vector and pressure fields at $t = 0.17$ (center) and at $t = 0.18$ (right). Symmetric stress tensor, **characteristics method**, coarse mesh, $\Delta t = 0.01$ and $p_{\text{in}}(t) = 10\sin(t)$. Velocity magnitude in 10^{-6} m^3/s and pressure in 10^{-1} Pa.

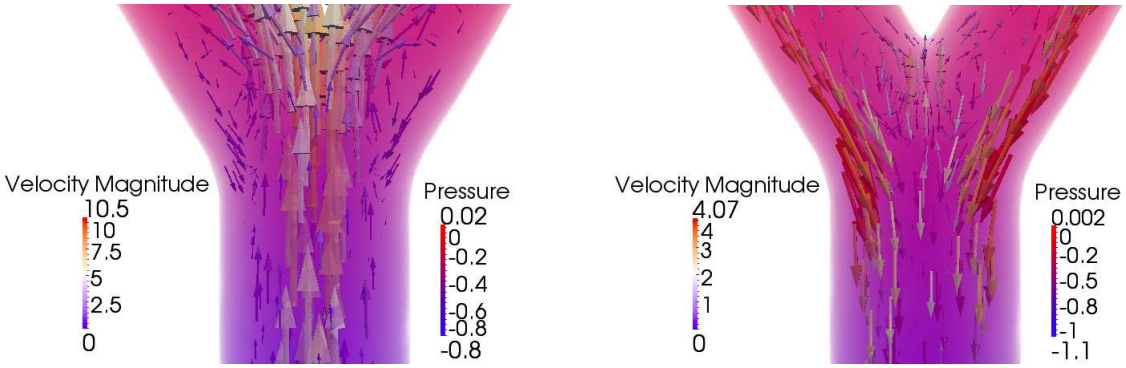

Figure 10: Velocity vector and pressure fields at $t = 3,23$ (left) and at $t = 3,25$ (right). Velocity magnitude in 10^{-6} m^3/s and pressure in 10^{-1} Pa.

3.3.3 A form which conserves the energy. (Formulation C, see Section 2.3.1)

In this section, we deal with the variational Problem P2.5. We consider the following discrete problem:

For each $t \in [0,T]$, seek $\mathbf{u}_h(t,\cdot) \in \mathbf{V}_h$ and $p_h(t,\cdot) \in M_h$ such that:

$$\begin{cases} \rho\left(\dfrac{\mathrm{d}}{\mathrm{d}t}\left(\mathbf{u}_h(t),\mathbf{v}_h\right) + b(\mathbf{u}_h(t),\mathbf{u}_h(t),\mathbf{v}_h) - (\mathbf{v}_h\cdot\nabla\mathbf{u}_h(t),\mathbf{u}_h(t))\right) & \\ \qquad +a(\mathbf{u}_h(t),\mathbf{v}_h) + d(\mathbf{v}_h,p_h^{\text{tot}}(t)) = \ell_{\text{in}}^{\text{tot}}(\mathbf{v}_h) + \ell_{\text{out}}^{\text{tot}}(\mathbf{v}_h), & \forall \mathbf{v}_h \in \mathbf{V}_h,\ t\in(0,T), \\ d(\mathbf{u}_h(t),q_h) = 0, & \forall q_h \in M_h,\ t\in(0,T), \\ \mathbf{u}_h(0) = \mathbf{u}_{0,h}, & \mathbf{u}_{0,h}\in\mathbf{V}_h. \end{cases}$$

We choose the following time discretization:

$$\begin{cases} \dfrac{\rho}{\Delta t}\left(\mathbf{u}_h^{n+1},\mathbf{v}_h\right)_\Omega + \rho\ b(\mathbf{u}_h^{n+1},\mathbf{u}_h^n,\mathbf{v}_h) - \rho(\mathbf{v}_h\cdot\nabla\mathbf{u}_h^n,\mathbf{u}_h^{n+1}) & \\ \qquad +a(\mathbf{u}_h^{n+1},\mathbf{v}_h) + d(\mathbf{v}_h,p_h^{\text{tot}}) = \dfrac{\rho}{\Delta t}\left(\mathbf{u}_h^n,\mathbf{v}_h\right)_\Omega + \ell_{\text{in}}^{\text{tot}}(\mathbf{v}_h) + \ell_{\text{out}}^{\text{tot}}(\mathbf{v}_h), & \forall \mathbf{v}_h\in\mathbf{V}_h, \\ d(\mathbf{u}_h,q_h) = 0, & \forall q_h\in M_h, \\ \mathbf{u}_h(0) = \mathbf{u}_{0,h}, & \mathbf{u}_{0,h}\in\mathbf{V}_h. \end{cases}$$

It is not more complicated than the basic formulation. However, the natural boundary conditions that are implicit with this formulation are not very satisfactory on a modeling point of view for the

problems that we have been considering. Indeed, we can observe in Figure 14 that we do not obtain a Poiseuille flow.

Test case: $\Delta t = 0.01$, symmetric tensor, $p_{\text{in}}(t) = 10\sin(t)$

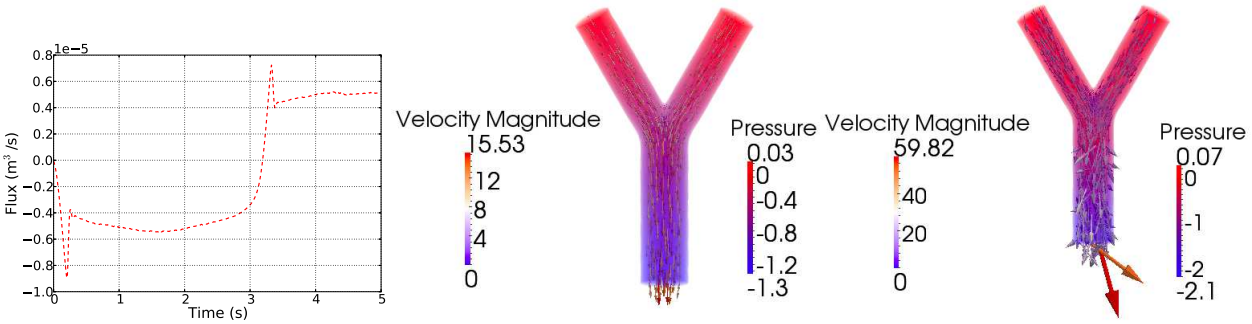

Figure 11: Left: flux (m^3/s) as a function of time (s) at the inlet. Center and right: velocity vector and pressure fields at $t = 3,27$ (center) and at $t = 3,34$ (right). Symmetric stress tensor, formulation of the convective term which conserves the energy, coarse mesh, $\Delta t = 0.01$ and $p_{\text{in}}(t) = 10\sin(t)$. Velocity magnitude in 10^{-6} m^3/s and pressure in 10^{-1} Pa.

In figure 11-left, we observe that the GMRES algorithm converges. However, the obtained solution is clearly not the right one (see Figure 11-right). The flux at the inlet (see Figure 11-left) has a poor agreement with the flux of the reference solution.

Test case: $\Delta t = 0.001$, nonsymmetric tensor, coarse mesh, $p_{\text{in}}(t) = \sin(t)$

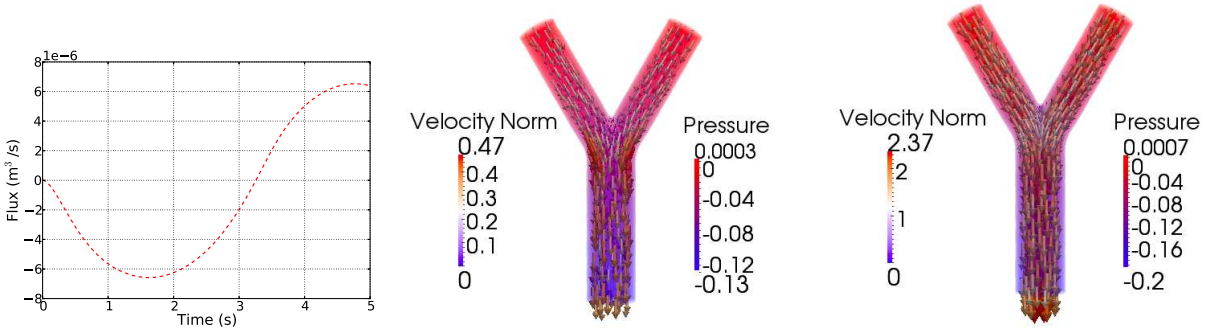

Figure 12: Left: flux (m^3/s) as a function of time (s) at the inlet. Center and right: velocity vector and pressure fields at $t = 3,27$ (center) and at $t = 3,34$ (right). Nonsymmetric stress tensor, formulation of the convective term which conserves the energy, coarse mesh, $\Delta t = 0.001$ and $p_{\text{in}}(t) = \sin(t)$. Velocity norm in 10^{-6} m^3/s and pressure in 10^{-1} Pa.

On Figure 12, we took a lower time-step and a lower inlet pressure. The computation is still stable (the GMRES converges). Moreover, the flux at the inlet (see Figure 12-left) is better than in the last test-case, it has a good agreement with the flux of the reference solution obtained with the characteristics method. On Figure 12-center-right, we observe that the solution has the right behaviour.

In Figure 13, we observe that the scheme allows to capture the vortices when the flow reverses. However, the eddies seem underperformed compared to the same computation with the method of characteristics.

Remark 3.4. A reversal flow occurs when the inspiration ends and the expiration begins.

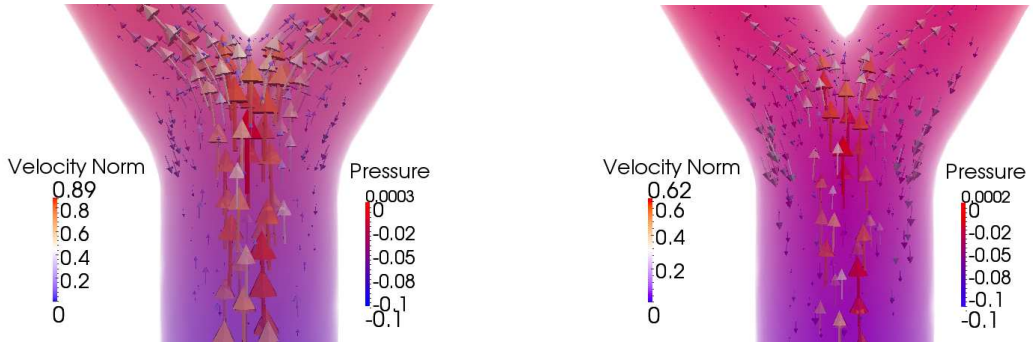

Figure 13: Velocity vector and pressure fields at $t = 3,25$ (left) and at $t = 3,258$ (right). Nonsymmetric stress tensor, formulation of the convective term which conserves the energy, coarse mesh, $\Delta t = 0.001$ and $p_{\text{in}}(t) = \sin(t)$. Velocity norm in 10^{-6} m^3/s and pressure in 10^{-1} Pa.

Test case: $\Delta t = 0.001$, nonsymmetric tensor, refined mesh, $p_{\text{in}}(t) = \sin(t)$

In this test-case, we refine the space-step: we take the refined mesh, with 102 thousand tetrahedra.

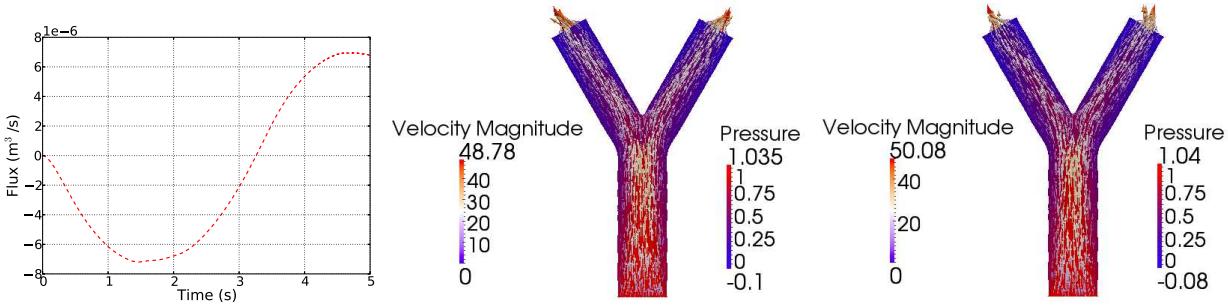

Figure 14: Left: flux (m^3/s) as a function of time (s) at the inlet. Center and right: velocity vector and pressure fields at $t = 1,504$ (center) and at $t = 1,508$ (right). Nonsymmetric stress tensor, formulation of the convective term which conserves the energy, refined mesh, $\Delta t = 0.001$ and $p_{\text{in}}(t) = \sin(t)$. Velocity magnitude in 10^{-6} m^3/s and pressure in 10^{-1} Pa.

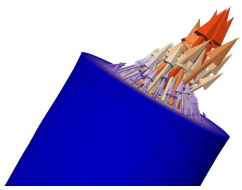

Figure 15: Zoom on one outlet of Figure 14-center.

On Figure 14, we observe that the GMRES has converged and that the behaviour of the flux at the entrance is the same that using the characteristics method, which can be considered like the reference. Moreover, the computation has converged. However, the velocity field at the outlets has not a good agreement with a Poiseuille flow, even with a low applied pressure which implies a low value of the term $\frac{\rho}{2}|\mathbf{u}|^2$. Indeed, the vectors are going towards the center of the mother tube, they are no longer orthogonal to the outlet (see Figure 15). Then this formulation does not seem the right one in a modeling point of view for our applications. Indeed, we truncate artificially the initial whole domain but the tube should actually extend and we should get a Poiseuille flow.

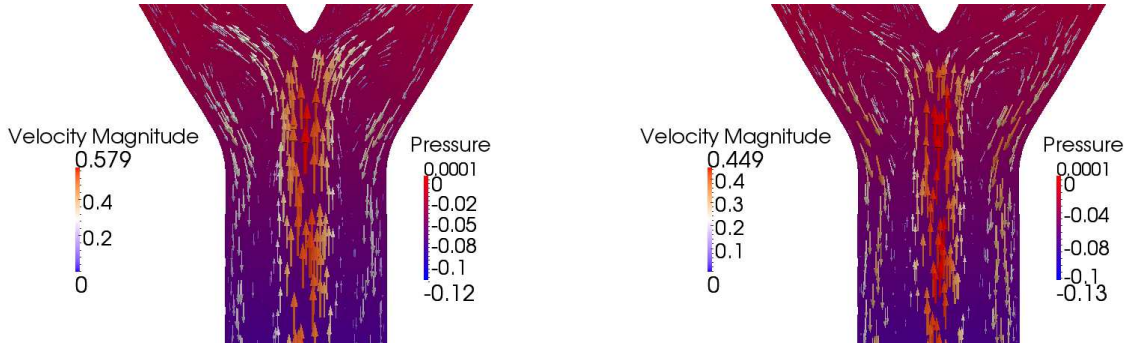

Figure 16: Velocity vector and pressure fields at $t = 3,264$ (left) and at $t = 3,267$ (right). Nonsymmetric stress tensor, formulation of the convective term which conserves the energy, $\Delta t = 0.001$ and $p_{\text{in}}(t) = \sin(t)$. Velocity magnitude in 10^{-6} m^3/s and pressure in 10^{-1} Pa.

On Figure 16, we observe that the velocity vector field has the right behaviour when the flow is reversing. The scheme satisfactorily captures the eddies.

3.3.4 Comparison between all the formulations, table of stability

We detailed the legend and the different meshes used in these tables in Section 3.1. The highlighted boxes match the test-cases shown in the last paragraphs. We compare the three forms of the convective term and the two forms of the viscous term, for different time-steps and mesh diameters. In the next tables, for the convective term, we note "Form. A" the basic form (see Section 3.3.1), "Form. B" the total derivative form (see Section 3.3.2), and "Form. C" the form which conserves the energy (see Section 3.3.3). For the viscous term, we note "$\mathbf{D}(\mathbf{u})$" the Cauchy tensor and "$\nabla\mathbf{u}$" the nonsymmetric form. We use a $\mathbb{P}_2/\mathbb{P}_1$ approximation here.

		0.01				0.001		
		Form. A	Form. B	Form. C		Form. A	Form. B	Form. C
5M	$\mathbf{D}(\mathbf{u})$	■	◯ √	⊠	$\mathbf{D}(\mathbf{u})$	■	◯ √	⊠
	$\nabla\mathbf{u}$	■	◯ ×	⊠	$\nabla\mathbf{u}$	■	◯ ×	⊠
		Form. A	Form. B	Form. C		Form. A	Form. B	Form. C
102M	$\mathbf{D}(\mathbf{u})$	■	◯ √	⊠	$\mathbf{D}(\mathbf{u})$	■	◯ √	⊠
	$\nabla\mathbf{u}$	■	◯ ×	⊠	$\nabla\mathbf{u}$	■	◯ ×	⊠
		Form. A	Form. B	Form. C		Form. A	Form. B	Form. C
309M	$\mathbf{D}(\mathbf{u})$	■	◯ √	⊠	$\mathbf{D}(\mathbf{u})$	■	◯ √	⊠
	$\nabla\mathbf{u}$	■	◯ √	⊠	$\nabla\mathbf{u}$	■	◯ √	⊠

Table 2: Comparison between all the formulations, for different time-steps and mesh diameters, with $p_{\text{in}} = 10\sin(t)$.

	0.01				0.001			
5M		Form. A	Form. B	Form. C		Form. A	Form. B	Form. C
	$\mathbf{D}(\mathbf{u})$	■	◯ √	☒	$\mathbf{D}(\mathbf{u})$	■	◯ √	◯ ×
	$\nabla\mathbf{u}$	■	◯ ×	☒	$\nabla\mathbf{u}$	■	◯ ×	◯ ×
102M		Form. A	Form. B	Form. C		Form. A	Form. B	Form. C
	$\mathbf{D}(\mathbf{u})$	◯ √	◯ √	☒	$\mathbf{D}(\mathbf{u})$	◯ √	◯√	◯ √
	$\nabla\mathbf{u}$	■	◯ ×	☒	$\nabla\mathbf{u}$	■	◯ √	◯√
309M		Form. A	Form. B	Form. C		Form. A	Form. B	Form. C
	$\mathbf{D}(\mathbf{u})$	◯ √	◯√	☒	$\mathbf{D}(\mathbf{u})$	◯ √	◯ √	◯ √
	$\nabla\mathbf{u}$	■	◯ √	☒	$\nabla\mathbf{u}$	◯ √	◯ √	◯√

Table 3: Comparison between all the formulations, for different time-steps and space-steps, with $p_{\text{in}} = \sin(t)$.

In Table 2 and Table 3, we observe that the characteristics method is stable from low time-step and from coarse meshes. However, one has to pay attention to the precision of the computation. Indeed, as we can see for small time-steps and coarse meshes, stability does not imply that the obtained solution has a good agreement with the reference solution. Here we compare the flux at the inlet/outlets. We note that the computations are more stable with lower applied pressures. For instance, with small data (see Table 3), the energy-preserving scheme gives a "good" solution (close to the reference solution) with lower time-step.

3.3.5 Conclusion

To sum up, the basic formulation (Formulation A) allows to get a Poiseuille profile at the outlets, it is suitable for our problem from a modeling point of view. However, it does not allow to bound the energy and then the existence and uniqueness theory is incomplete. It leads to unstable numerical solutions.

The formulation using the total derivative and the method of characteristics to discretize it is much more stable. It allows to consider higher applied pressure and to get good numerical solutions with a not too much refined mesh and with a reasonable time-step. However, the treatment of natural boundary conditions may induce some stabilizations that we have not understood until now. To finish, from a scientific computing point of view, the method has a drawback: to solve the system with a parallel computing does not bring reduction of the computational cost. Indeed, the different processors should communicate a lot to backtrack the characteristic lines for each vertex.

The energy-preserving formulation allows to get stable numerical solutions. We get them with finer meshes than with the total derivative method. However, one can easily use a parallel algorithm to solve the systems. Then the computational cost is not higher. On a modeling point of view, this formulation does not allow to get a Poiseuile profile at the outlets.

3.4 Stabilization methods

3.4.1 Added term to match the discrete and the continuous energy balance

As said before, when the problem is space-discretized, the divergence is no more zero. Then we can add a term consistent with the continuous solution so that the discrete energy balance matches the

continuous one. In the energy balance, integrating by parts the convective term, we obtain the kinetic energy flow:

$$\int_\Omega (\mathbf{u}\cdot\nabla\mathbf{u})\cdot\mathbf{u} = \int_{\partial\Omega}\frac{|\mathbf{u}|^2}{2}\mathbf{u}\cdot\mathbf{n} - \int_\Omega \frac{|\mathbf{u}|^2}{2}\nabla\cdot\mathbf{u}.$$

If we semi-discretized it in time, we get:

$$\frac{\rho}{2}\int_\Omega \mathbf{u}^n\cdot\nabla|\mathbf{u}^{n+1}|^2 = \underbrace{\frac{\rho}{2}\int_{\partial\Omega}(\mathbf{u}^n\cdot\mathbf{n})|\mathbf{u}^{n+1}|^2}_{\text{kinetic energy flow}} - \underbrace{\frac{\rho}{2}\int_\Omega(\nabla\cdot\mathbf{u}^n)|\mathbf{u}^{n+1}|^2}_{=0 \text{ if exact solution}}.$$

Then we add in the variational form:

$$\frac{\rho}{2}\int_\Omega(\nabla\cdot\mathbf{u}^n)\mathbf{u}^{n+1}\mathbf{v}$$

to match the discrete and the continuous energy balance. Note that this term does not modify the consistence. This method comes from [68].

3.4.2 Stabilized finite elements and transport-dominant flows

Treating dominant transport with residual-based stabilizations. When one is considering the Navier–Stokes equations, in the case of high Reynolds numbers (for instance $Re > 500$ for the two-dimensional driven cavity, or $Re > 50$ for pipe-flow around a cylinder), that is to say when the flow is advective-dominant, the finite element approaches detailed in Section 3.3.1 may become unstable since they essentially use central-differences-like discretization of the convective term, and then need a mesh fine enough. This instability most frequently occurs in form of a slow-down or even break-down of the iteration processes for solving the algebraic problems.

In order to avoid these effects, some additional numerical damping is required.Then by modifying the discretization, one enhances its coercivity, and thereby increases its stability.

The idea of the so-called "streamline diffusion method" is to introduce artificial diffusion acting only in the transport direction while maintaining the strong consistency of the scheme.

Then we consider the problem:

$$\begin{cases}\text{Find } \mathbf{u}\in\mathbf{V}=\mathbf{H}_0^1(\Omega) \text{ such that}\\ a(\mathbf{u},\mathbf{v}) = F(\mathbf{v}),\ \forall\mathbf{v}\in\mathbf{V}\end{cases}$$

and the discrete scheme:

$$\begin{cases}\text{Find } \mathbf{u}_h\in\mathbf{V}_h \text{ such that}\\ a_h(\mathbf{u}_h,\mathbf{v}_h) = F(\mathbf{v}_h),\ \forall\mathbf{v}_h\in\mathbf{V}_h\end{cases}$$

with $\mathbf{V}_h\subset\mathbf{V}$ a conforming finite element space that consists of piecewise polynomials of degree k, i.e.

$$\mathbf{V}_h = \{\mathbf{v}_h\in\mathbf{V}\ :\ \mathbf{v}_h|_K\in P_k(K) \text{ for all } K\in\mathcal{T}_h\}$$

and with $a_h(\mathbf{u}_h,\mathbf{v}_h) = a(\mathbf{u}_h,\mathbf{v}_h) + g_h(\mathbf{u}_h,\mathbf{v}_h)$. We note $\mathcal{L}$ the linear operator associated with the bilinear form a. This kind of methods is strongly consistent with the initial problem. Indeed, if $\mathbf{u}$ the solution of the initial problem is supposed to be regular (in the sense that $\mathcal{L}\mathbf{u} = f$ in $L^2(K)\ \forall K\in\mathcal{T}_h$), we have $g_h(\mathbf{u},\mathbf{v}_h) = 0\ \forall\mathbf{v}\in V_h$. Moreover, they still allow to have the error estimates of the Galerkin

method. To decompose $\mathcal{L}$, we can consider its symmetric part $\mathcal{L}_S$ and its skew-symmetric one $\mathcal{L}_{SS}$. Then the bilinear form can be written as $a_h(\mathbf{u}_h, \mathbf{v}_h) = a(\mathbf{u}_h, \mathbf{v}_h) + g_h(f; \mathbf{u}_h, \mathbf{v}_h)$ with:

$$g_h(f; \mathbf{u}_h, \mathbf{v}_h) = \sum_{K \in \mathcal{T}_h} \tau_K(h) \int_K (\mathcal{L}\mathbf{u}_h - f) \cdot (\mathcal{L}_{SS} + \gamma \mathcal{L}_S)\mathbf{v}$$

with $\tau_K(h) > 0$ the stabilization parameter. Then the standard Galerkin method is augmented by the addition of terms that represent the residual of the original differential equation on each mesh element.

Among these methods, the GALS one (Galerkin/Least Square) is obtained with $\gamma = 1$, the SUPG one (Streamline Upwind/Petrov-Galerkin) with $\gamma = 0$ and the DWG one (Douglas-Wang/Galerkin) with $\gamma = -1$.

The method is conceptually simple but has two main defects:

1. Its implementation needs a modification of the linear system $Ax = b$. With the method, we have to solve $(A + G_h)x = b + \widetilde{g}_h$, with G_h a nonsymmetric matrix [63].
2. There is no optimal choice of $\tau_K(h)$ (which is often a "user-specified" quantity, see [18]), and the method may be too diffusive (and then non-accurate) if one chooses a large value parameter [61].

For an analysis of these strongly consistent methods and more details on the "user-specified" parameter, we refer to Sections 8.3 and 8.4 of [63] and to Section 3.2 of [64].

Stokes problem and finite elements which do not satisfy the inf-sup condition. When we consider a Stokes problem (with Dirichlet boundary conditions on the boundaries, i.e. the velocity is specified everywhere on the boundary) and its variational formulation, it is well known that this problem is ill-posed. In a discrete framework, if one chooses some finite elements for the velocity and the pressure which satisfy the discrete inf-sup condition, we obtain the uniqueness of the weak pressure (see [19]). Using some illustrations with several choices of stable mixed approximation methods, [18] presents a methodology for establishing inf–sup stability. For instance, one can use a $\mathbb{P}_2/\mathbb{P}_1$ approximation, i.e. a quadratic approximation for the velocity components and a linear one for the pressure.

However, one may be interested in using unstable finite elements, i.e. for instance the lowest order mixed approximation methods, based on globally continuous linear approximation for velocity components, together with a continuous linear pressure ($\mathbb{P}_1/\mathbb{P}_1$). Indeed, they imply a lower computational cost. However, the inf-sup condition is no satisfied anymore available and the problem is again ill-posed. However, a residual-based stabilization used to deal with a transport-dominant flow can be applied to the ill-posed Stokes problem and then stabilize the finite elements.

One has to find suitable values of the parameters to guarantee both stability and convergence, with respect to a suitable norm. See [26] and Section 3.2 of [64].

Remark 3.5. The streamline diffusion method is obtained using test functions of the form $\mathcal{L}\mathbf{v}$ where $\mathbf{v} \in \mathbf{V}_h$. Then test functions are not chosen in the functional space where the discrete solution $\mathbf{u}_h$ is sought. Such a method is called Petrov-Galerkin method. In a standard Galerkin method, the spaces of trial and test functions are the same.

To sum up, these methods can be applied to different problems in order to cure different kinds of pathologies. Indeed, they overcome the instabilities related to the discrete inf-sup incompatibility or to the presence of dominant convection.

Table of stability for the streamline diffusion method. We have seen that considering the approximation of the Navier–Stokes equations, the onset of instabilities is due either to large advection or to the presence of wrong pressure modes (when the discrete inf-sup condition is not verified). Thus the use of a residual-based stabilization may solve these two kinds of problems.

In this section, we solve the system detailed in Section 3.3.1, with a $\mathbb{P}_1/\mathbb{P}_1$ approximation. To use a residual-based stabilization (see e.g. [71, 72]), we add the term:

$$
\begin{aligned}
&g_h(f;\mathbf{u}_h,\mathbf{v}_h;p_h,q_h) = \\
&\quad \sum_{K\in\mathcal{T}_h}\int_K \frac{1}{\rho}\tau_{1,K}(h)[\rho\mathbf{u}_h\cdot\nabla\mathbf{v}_h+\nabla\cdot\boldsymbol{\sigma}(q_h,\mathbf{v}_h)]\cdot(\rho(\partial_t\mathbf{u}_h+\mathbf{u}_h\cdot\nabla\mathbf{u}_h)+\nabla\cdot\boldsymbol{\sigma}(p_h,\mathbf{u}_h)-f) \\
&\qquad + \sum_{K\in\mathcal{T}_h}\rho\tau_{2,K}(h)\int_K(\nabla\cdot\mathbf{u}_h,\nabla\cdot\mathbf{v}_h)
\end{aligned}
$$

in the formulation, with

$$
\tau_{2,K}(h)=0,\ \ \tau_{1,K}(h)=\frac{\tau}{\sqrt{\dfrac{4}{\Delta t^2}+\dfrac{4|\mathbf{u}|^2}{h^2}+\dfrac{16\eta^2}{\rho^2h^4}}},
$$

with $\tau = 0.1,\ 0.6$ and 1. This term is strongly consistent with the initial problem. Then $\Delta\mathbf{u}_h$ and $\Delta\mathbf{v}_h$ are zero.

Remark 3.6. The streamline diffusion stabilizes the dominant transport. Then instabilities linked to natural boundary conditions decrease. However, the method is difficult to use when one chooses $\mathbb{P}_2/\mathbb{P}_1$ approximation: assemble a Laplacian term and compute the parameters.

We detail the legend used in these tables in the Paragraph 3.1. Here we have $p_{\text{in}} = \sin(t)$.

	0.01			0.001				0.000 1			
5M		0.01	0.06	0.1		0.01	0.06	0.1		0.01	0.06	0.1
	$\mathbf{D}(\mathbf{u})$	🟥	🟢	🟢	$\mathbf{D}(\mathbf{u})$	🟥	🟥	⊠	$\mathbf{D}(\mathbf{u})$	🟥	🟥	⊠
	$\nabla\mathbf{u}$	🟥	🟢	🟢	$\nabla\mathbf{u}$	🟥	🟥	🟢	$\nabla\mathbf{u}$	🟥	🟥	🟥
50M		0.01	0.06	0.1		0.01	0.06	0.1		0.01	0.06	0.1
	$\mathbf{D}(\mathbf{u})$	🟥	🟢	🟢	$\mathbf{D}(\mathbf{u})$	🟢	🟢	🟢	$\mathbf{D}(\mathbf{u})$	🟢	🟢	🟢
	$\nabla\mathbf{u}$	🟥	🟢	🟢	$\nabla\mathbf{u}$	🟢	🟢	🟢	$\nabla\mathbf{u}$	🟥	🟢	🟢

Table 4: Comparison between different values of the τ parameter, for different time-steps and space-steps, with $p_{\text{in}} = \sin(t)$.

One has to choose carefully the user-specified parameter. Indeed, we note in Table 4 that for the same time-step and the same mesh, if the parameter is not high enough, we do not obtain a stable solution. However, a too large parameter introduces an excessive diffusion.

We observe that for the same time-step, the computation stability is reached with a smaller parameter if the mesh is fine enough.

To sum up, one has to pay attention to not introduce too much diffusion if there is no need to.

3.4.3 Balance the flow of kinetic energy, adding a term in the normal constraint

In some papers (see e.g. [49, 31]), the authors managed to compute flows with the basic formulation detailed in Section 3.3.1 and with Neumann boundary conditions. However, this approach seems to be linked to the use of very small data, in particular for the pressure at the inlet. Once one takes a larger pressure, some instabilities occur, making divergent the GMRES algorithm, see for instance Figure 5. In this section, we detail the method mentioned in Remark 2.6, which leads to stable computation using the basic formulation and Neumann boundary conditions, as showed in the next numerical cases.

As explained in Remark 2.6, one can overcome the lack of energy conservation by adding a term to remove the flow of kinetic energy at the boundaries. Then we add this stabilizing term in the formulation (boundary term), see [20]:

$$-\beta \, \frac{\rho}{2} \int_{\Gamma_{\text{out}}} (\mathbf{u}^n \cdot \mathbf{n})_- (\mathbf{u}^{n+1} \cdot \mathbf{v})$$

where $\beta \in [0, 1]$ and where $(\mathbf{u}^n \cdot \mathbf{n})_-$ is defined as

$$(\mathbf{u}^n \cdot \mathbf{n})_- = \frac{\mathbf{u}^n \cdot \mathbf{n} - |\mathbf{u}^n \cdot \mathbf{n}|}{2} = \begin{cases} \mathbf{u}^n \cdot \mathbf{n} & \text{if } \mathbf{u}^n \cdot \mathbf{n} < 0, \\ 0 & \text{otherwise.} \end{cases}$$

It has some advantages: accuracy, robustness, it is easy to implement, and there is no additional computational cost. It has also some disadvantages: β is an adjustable parameter, and the method can change the local dynamics, but these effects are reported as negligible in [20]. From a physical point of view, the added term is an outward traction, opposite the direction of backflow, which pushes the flow in the direction of the outward normal. This term provides the "missing" convective flow information from outside of the computational domain during flow reversal. It is also useful when backflow phenomena occur in blood physical flow. Indeed, in these cases, the applied pressures are pulses, and a partial flow reversal can occur at the boundaries. This method is often used in blood flow computations, see e.g. [75].

Actually, the idea was proposed in [9] and in [6] for theoretical purpose (see Remark 2.6). We refer also to [41]. It consists in modifying the Neumann boundary condition $\eta \nabla \mathbf{u} \cdot \mathbf{n} - p\mathbf{n} = -p_\alpha \mathbf{n}$ as:

$$\eta \nabla \mathbf{u} \cdot \mathbf{n} - p\mathbf{n} = -\overline{p}_\alpha \mathbf{n} - \beta \frac{\rho}{2} (\mathbf{u} \cdot \mathbf{n})_- \mathbf{u}.$$

In [20], the authors choose $\overline{p}_\alpha = p_\alpha$. A similar method is described in [31], except that in this paper, the authors choose $\overline{p}_\alpha = p_\alpha + \frac{\rho}{2} f(\mathbf{u}_{\text{ref}}, Q_{\text{ref}})$, with $f(\mathbf{u}_{\text{ref}}, Q_{\text{ref}})$ an approximation of $(\mathbf{u}^n \cdot \mathbf{n})_- \mathbf{u}$ based on an given velocity profile $\mathbf{u}_{\text{ref}}$ and a given flux Q_{ref}. Then, both pressure and flow rates are imposed.

In these kinds of stabilization, the aim is to suppress the kinetic energy flux. According to the parameter β, we are cancelling all the undesirable term or only a part of it. The more we compensate the term (β is high), the further away the "right" behaviour of the solution.

Remark 3.7. The aim of the formulation seen in Section 2.3.1 is also to control the kinetic energy flux. However, using this formulation, all the flux of kinetic energy is controlled, as applying boundary conditions of Remark 2.6 ($\beta = 1$ in the previous stabilization method). Then the basic formulation stabilized with a small β should be better for our problem in a modeling point of view, since it leads to a velocity field close to the expected Poiseuile flow.

Test case: $\Delta t = 0.01$, nonsymmetric tensor, $p_{\text{in}} = 10\sin(t)$, $\beta = 1$

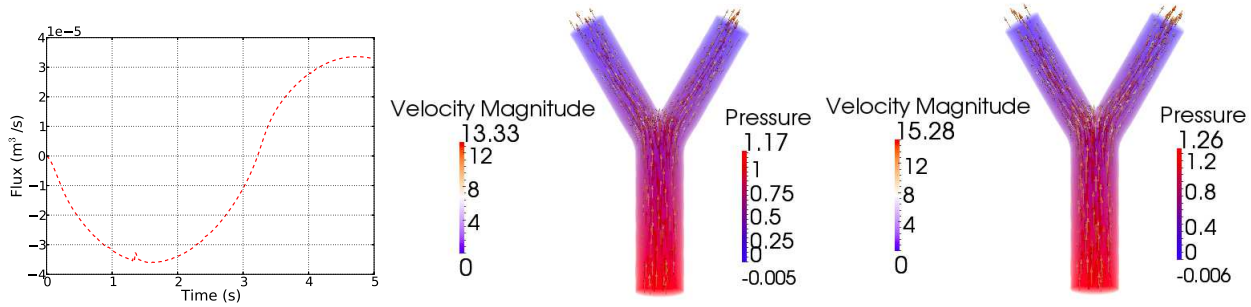

Figure 17: Left: flux (m^3/s) as a function of time (s) at the inlet. Center and right: velocity vector and pressure fields at $t = 0.12$ (center) and at $t = 0.13$ (right). Nonsymmetric stress tensor, basic formulation of the convective term, coarse mesh, $\Delta t = 0.01$ and $p_{\text{in}}(t) = 10\sin(t)$. With stabilization described in Section 3.4, $\beta = 1$. Velocity magnitude in 10^{-6} m^3/s and pressure in 10^{-1} Pa.

In Figure 17, we observe that the adding term makes the computation stable (there is no oscillation that could make a break-down of the iteration processes for solving the algebraic problems).

Test case: $\Delta t = 0.01$, symmetric tensor, $p_{\text{in}}(t) = 10\sin(t)$, $\beta = 1$

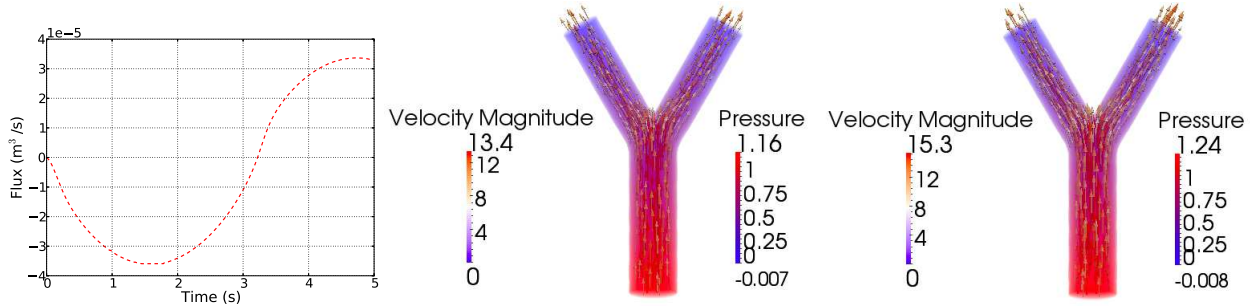

Figure 18: Left: flux (m^3/s) as a function of time (s) at the inlet. Center and right: velocity vector and pressure fields at $t = 0.12$ (center) and at $t = 0.13$ (right). Symmetric stress tensor, basic formulation of the convective term, coarse mesh, $\Delta t = 0.01$ and $p_{\text{in}}(t) = 10\sin(t)$. With stabilization described in Section 3.4, $\beta = 1$. Velocity magnitude in 10^{-6} m^3/s and pressure in 10^{-1} Pa.

In Figure 18, we have used the symmetric tensor. We observe also that the adding term makes the computation stable.

Test case: $\Delta t = 0.01$, symmetric tensor, $p_{\text{in}}(t) = 10\sin(t)$, $\beta = 0.2$

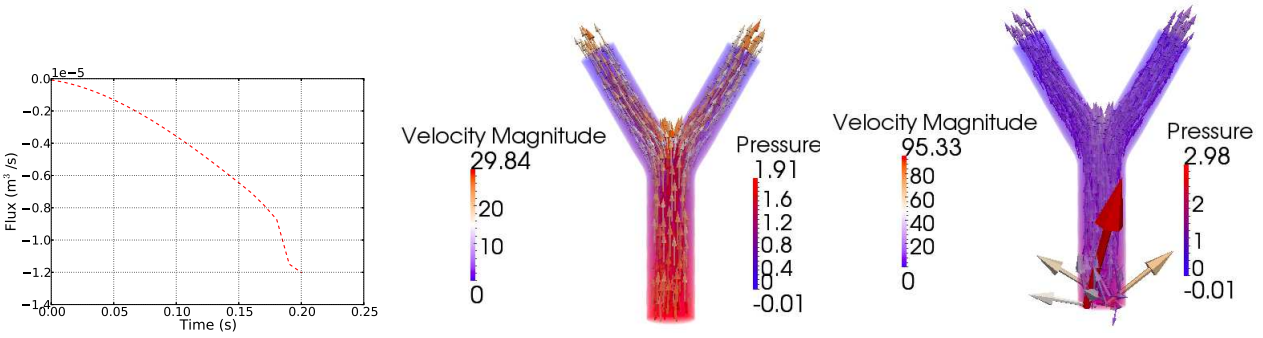

Figure 19: Left: flux (m^3/s) as a function of time (s) at the inlet. Center and right: velocity vector and pressure fields at $t = 0.19$ (center) and at $t = 0.2$ (right). Symmetric stress tensor, basic formulation of the convective term, coarse mesh, $\Delta t = 0.01$ and $p_{\text{in}}(t) = 10\sin(t)$. With stabilization described in Section 3.4, $\beta = 0.2$. Velocity magnitude in 10^{-6} m^3/s and pressure in 10^{-1} Pa.

In Figure 19, we have used the same method but with a lower β parameter. The adding term makes the computation more stable than without (the computation goes further than in Figure 5). However, it is not sufficient to get a convergent GMRES algorithm.

Remark 3.8. These method can also solve another problem encountered at the outlets when one considers tidal flows (blood flow in arteries for instance). As: flow partially or completely reverses, the outlets become partial or complete inlets. Partial retrograde flow can also arise because of flow recirculation induced by the bifurcating nature of the geometry. Complete reversal of the flow direction occurs, for example, in airflow simulations during the expiratory phase.

Table of stability for different stabilizations. We detail the legend used in these tables in the Paragraph 3.1. Here we have $p_{\text{in}} = 10\sin(t)$.

		0.01				0.001		
		0.2	0.6	1		0.2	0.6	1
5M	$\mathbf{D(u)}$	■	■	○	$\mathbf{D(u)}$	■	○	○
	$\nabla\mathbf{u}$	■	■	○	$\nabla\mathbf{u}$	■	○	○
		0.2	0.6	1		0.2	0.6	1
102M	$\mathbf{D(u)}$	■	○	○	$\mathbf{D(u)}$	■	○	○
	$\nabla\mathbf{u}$	■	○	○	$\nabla\mathbf{u}$	■	○	○

Table 5: Comparison between different values of the β parameter, for different time-steps and space-steps, with $p_{\text{in}} = 10\sin(t)$.

As said for the residual-based stabilizations, one has to choose carefully the user-specified parameter β. Indeed, we observe in Table 5 that the higher is β, the more the solution is far from the expected flow. But if the parameter is too low, the kinetic energy injected into the system is too high, which implies the no-convergence of the computation.

We observe that for the same time-step, the computation convergence is reached with a smaller parameter if the mesh is fine enough. One has to pay attention to not constraint too much the flux of kinetic energy if there is no need to in order to not modify too much the computation with the stabilization method.

3.5 Comparison between the different stabilization methods

In Figure 20, we gather the flux at the entrance obtained throughout the paper. In Figure 21, we do the same but with test-cases involving higher inlet pressures. If one uses the stabilization detailed in Section 3.4.3 with a too high β parameter, there is a poor agreement between the obtained solution and the others. Stability is thus achieved at the expense of accuracy. This method can modify a lot the solution whereas the streamline diffusion method and the characteristics method lead to similar numerical solutions. Actually, we assume that the characteristics method introduce a diffusion along the characteristic lines, as using the streamline diffusion method.

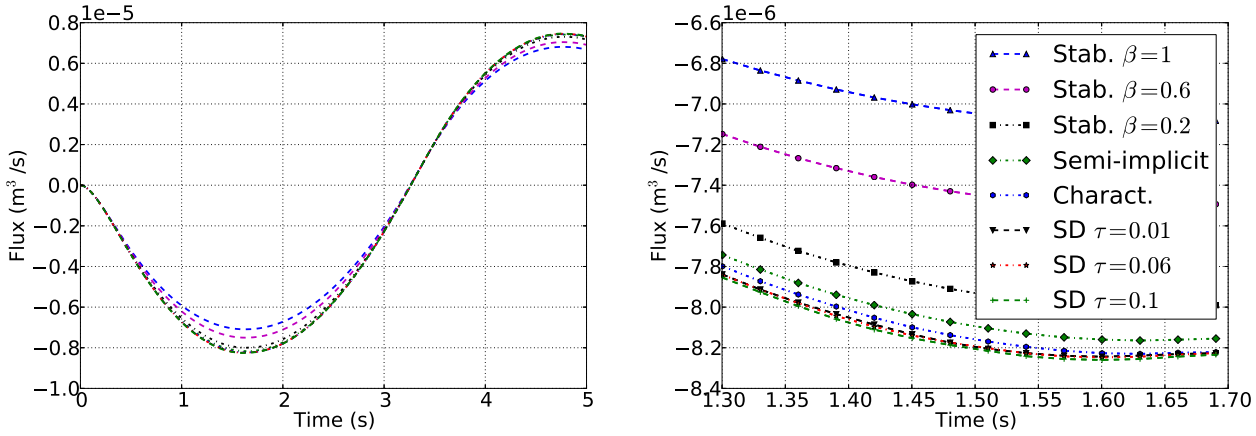

Figure 20: Flux (m^3/s) as a function of time (s) at the inlet, for different schemes: Formulation A with the semi-implicit treatment with $\mathbb{P}_2/\mathbb{P}_1$ finite elements ("Semi-implicit"), with additional stabilization term (see Section 3.4.3) with different β parameters ("Stab. β = ..."), with $\mathbb{P}_1/\mathbb{P}_1$ finite elements with a streamline diffusion method (see Section 3.4.2) for different parameters τ ("SD τ = ...") and Formulation B ("Charact."). Symmetric stress tensor, refined mesh, $\Delta t = 0.001$ and $p_{\text{in}}(t) = \sin(t)$.

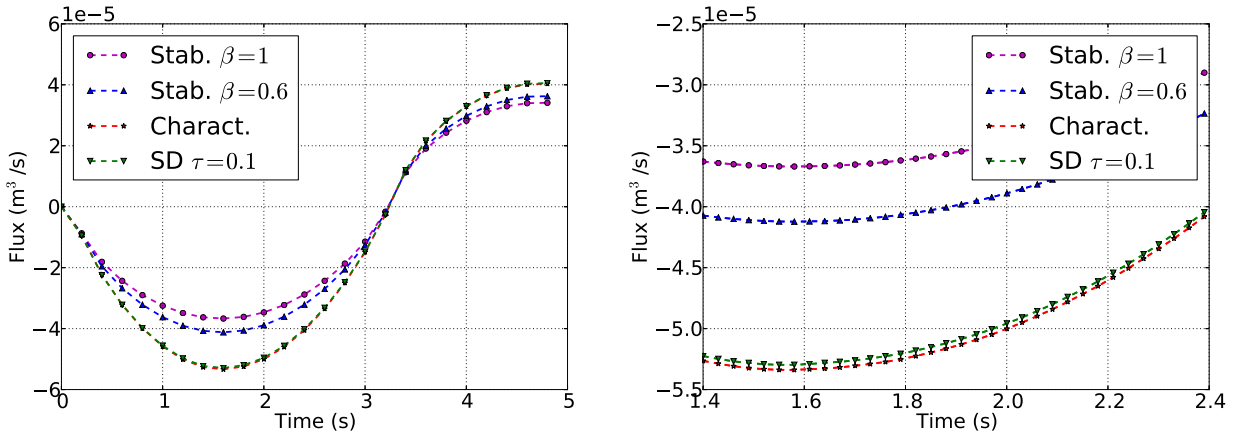

Figure 21: Flux (m^3/s) as a function of time (s) at the inlet, for different schemes: Formulation A with the semi-implicit treatment with $\mathbb{P}_2/\mathbb{P}_1$ finite elements with additional stabilization term (see Section 3.4.3) with different β parameters ("Stab. β = ..."), with $\mathbb{P}_1/\mathbb{P}_1$ finite elements with a streamline diffusion method (see Section 3.4.2) for $\tau = 0.1$ ("SD τ = 0.1") and Formulation B ("Charact."). Symmetric stress tensor, refined mesh, $\Delta t = 0.001$ and $p_{\text{in}}(t) = 10\sin(t)$.

4 Conclusion

In this paper, we have dealt with the Navier–Stokes equations in truncated domains. The subsequent introduction of artificial boundaries leads to the definition of suitable boundary conditions in order to preserve the physics of the flow. We are interested in biological applications, like flows in large blood arteries or in pulmonary airways. In these cases, the system is driven by physical pressures (the cardiac or alveoli pressures). We have reviewed different formulations of the Navier–Stokes equations, and we have investigated the existence and uniqueness theory when one applies boundary conditions involving the pressure. On a numerical point of view, these difficulties are still there: as suggested by the theory, we observed that when applying too high pressures and using the Formulation A (see Section 3.3.1), the iterative method treating the nonlinearities (a GMRES algorithm) does not converge anymore and leads to a blow up of the solution. To finish, we reviewed different methods to stabilize the systems, based on streamline diffusion (see Section 3.4.2) or direct handling of kinetic energy fluxes (see Section 3.4.3), and we illustrated that we must be careful with these methods which involve "user-specified" parameters.

Acknowledgements

The author wants to thank Céline Grandmont and Sébastien Martin for valuable discussions and for their very helpful feedbacks on the manuscript, and Bertrand Maury for his fruitful remarks. The present work has been partially supported by the Agence Nationale de la Recherche (ANR) through the projects ANR-11-TECS-006 (OxHelease) and ANR-08-JCJC-013-01 (M3RS).

References

[1] L. Baffico, C. Grandmont, and B. Maury. Multiscale modeling of the respiratory tract. *Mathematical Models & Methods in Applied Sciences*, 20(1):59–93, 2010.

[2] C. Bardos, M. Bercovier, and O. Pironneau. The vortex method with finite elements. *Mathematics of Computation*, 36(153):119–136, 1981.

[3] W. L. Barth and G. F. Carey. On a boundary condition for pressure-driven laminar flow of incompressible fluids. *International Journal for Numerical Methods in Fluids*, 54(11):1313–1325, 2007.

[4] J. M. Bernard. Time-dependent Stokes and Navier–Stokes problems with boundary conditions involving pressure, existence and regularity. *Nonlinear Analysis. Real World Applications*, 4(5):805–839, 2003.

[5] F. Billy, B. Ribba, O. Saut, H. Morre-Trouilhet, T. Colin, D. Bresch, J.-P. Boissel, E. Grenier, and J.-P. Flandrois. A pharmacologically based multiscale mathematical model of angiogenesis and its use in investigating the efficacy of a new cancer treatment strategy. *Journal of Theoretical Biology*, 260(4):545–562, 2009.

[6] F. Boyer and P. Fabrie. Outflow boundary conditions for the incompressible non-homogeneous Navier–Stokes equations. *Discrete and Continuous Dynamical Systems, Series B*, 7(2):219–250, 2007.

[7] F. Brezzi. On the existence, uniqueness and approximation of saddle-point problems arising from Lagrangian multipliers. *Rev. Française Automat. Informat. Recherche Opérationnelle Sér. Rouge*, 8(R-2):129–151, 1974.

[8] C.-H. Bruneau. Boundary conditions on artificial frontiers for incompressible and compressible Navier–Stokes equations. *ESAIM: Mathematical Modelling and Numerical Analysis*, 34(02):303–314, 2000.

[9] C.-H. Bruneau and P. Fabrie. New efficient boundary conditions for incompressible Navier–Stokes equations : a well-posedness result. *ESAIM: Mathematical Modelling and Numerical Analysis - Modélisation Mathématique et Analyse Numérique*, 30(7):815–840, 1996.

[10] C. Bègue, C. Conca, F. Murat, and O. Pironneau. À nouveau sur les équations de Stokes et de Navier–Stokes avec des conditions aux limites sur la pression. *Comptes Rendus des Séances de l'Académie des Sciences. Série I. Mathématique*, 304(1):23–28, 1987.

[11] C. Bègue, C. Conca, F. Murat, and O. Pironneau. Les équations de Stokes et de Navier–Stokes avec des conditions aux limites sur la pression. In *Nonlinear partial differential equations and their applications. Collège de France Seminar, Vol.\ IX (Paris, 1985–1986)*, volume 181 of *Pitman Res. Notes Math. Ser.*, pages 179–264. Longman Sci. Tech., Harlow, 1988.

[12] A. J. Chorin. Numerical solution of the Navier–Stokes equations. *Mathematics of Computation*, 22(104):745–762, 1968.

[13] F. Clavica, J. Alastruey, S. J. Sherwin, and A. W. Khir. One-dimensional modelling of pulse wave propagation in human airway bifurcations in space–time variables. In *Engineering in Medicine and Biology Society, 2009. EMBC 2009. Annual International Conference of the IEEE*, pages 5482–5485, 2009.

[14] T. Colin, A. Iollo, D. Lombardi, and O. Saut. Prediction of the evolution of thyroidal lung nodules using a mathematical model. *ERCIM News*, Special Issue "Computational Biology"(82), 2010.

[15] C. Conca, F. Murat, and O. Pironneau. The Stokes and Navier–Stokes equations with boundary conditions involving the pressure. *Japanese Journal of Mathematics. New Series*, 20(2):279–318, 1994.

[16] C. Conca, C. Parés, O. Pironneau, and M. Thiriet. Navier–Stokes equations with imposed pressure and velocity fluxes. *International Journal for Numerical Methods in Fluids*, 20(4):267–287, 1995.

[17] A.-C. Egloffe. *Étude de quelques problèmes inverses pour le système de Stokes. Application aux poumons.* PhD thesis, Université Pierre et Marie Curie, 2012.

[18] H. Elman, D. Silvester, and A. Wathen. *Finite elements and fast iterative solvers: with applications in incompressible fluid dynamics.* Oxford University Press, 2005.

[19] A. Ern and J.-L. Guermond. *Theory and practice of finite elements.* Springer, New York, 2004.

[20] M. Esmaily Moghadam, Y. Bazilevs, T.-Y. Hsia, I. E. Vignon-Clementel, A. L. Marsden, and Modeling of Congenital Hearts Alliance (MOCHA) Investigators. A comparison of outlet boundary treatments for prevention of backflow divergence with relevance to blood flow simulations. *Computational Mechanics*, 48(3):277–291, 2011.

[21] M. Esmaily Moghadam, F. Migliavacca, I. E. Vignon-Clementel, T.-Y. Hsia, A. Marsden, and Modeling of Congenital Hearts Alliance (MOCHA) Investigators. Optimization of shunt placement for the norwood surgery using multi-domain modeling. *Journal of Biomechanical Engineering*, 134(5):051002, 2012.

[22] M. Esmaily Moghadam, I. E. Vignon-Clementel, R. Figliola, and A. L. Marsden. A modular numerical method for implicit 0D/3D coupling in cardiovascular finite element simulations. *Journal of Computational Physics*, 244(0):63–79, 2012.

[23] FELiScE. INRIA forge project FELiScE : felisce.gforge.inria.fr, 2013.

[24] L. Formaggia, J.-F. Gerbeau, F. Nobile, and A. Quarteroni. Numerical treatment of defective boundary conditions for the Navier–Stokes equations. *SIAM Journal on Numerical Analysis*, 40(1):376–401, 2002.

[25] L. Formaggia, D. Lamponi, and A. Quarteroni. One-dimensional models for blood flow in arteries. *Journal of Engineering Mathematics*, 47(3-4):251–276, 2003.

[26] L. P. Franca and S. L. Frey. Stabilized finite element methods: II. the incompressible Navier–Stokes equations. *Computer Methods in Applied Mechanics and Engineering*, 99(2–3):209–233, 1992.

[27] T. Gemci, V. Ponyavin, Y. Chen, H. Chen, and R. Collins. Computational model of airflow in upper 17 generations of human respiratory tract. *Journal of Biomechanics*, 41(9):2047 – 2054, 2008.

[28] T. Gengenbach, V. Heuveline, and M. J. Krause. Numerical simulation of the human lung: A two–scale approach. *EMCL Preprint Series*, 11, 2011.

[29] C. Grandmont, Y. Maday, and B. Maury. A multiscale/multimodel approach of the respiration tree. In *New trends in continuum mechanics*, volume 3 of *Theta Ser. Adv. Math.*, pages 147–157. Theta, Bucharest, 2005.

[30] C. Grandmont, B. Maury, and A. Soualah. Multiscale modelling of the respiratory track: a theoretical framework. *ESAIM: Proceedings*, 23:10–29, 2008.

[31] V. Gravemeier, A. Comerford, L. Yoshihara, M. Ismail, and W. A. Wall. A novel formulation for Neumann inflow boundary conditions in biomechanics. *International Journal for Numerical Methods in Biomedical Engineering*, 28(5):560–573, 2012.

[32] P. M. Gresho. Incompressible fluid dynamics: some fundamental formulation issues. *Annual Review of Fluid Mechanics*, 23(1):413–453, 1991.

[33] P. M. Gresho. Some current CFD issues relevant to the incompressible Navier–Stokes equations. *Computer Methods in Applied Mechanics and Engineering*, 87(2):201–252, 1991.

[34] P. M. Gresho and R. L. Sani. On pressure boundary conditions for the incompressible Navier–Stokes equations. *International Journal for Numerical Methods in Fluids*, 7(10):1111–1145, 1987.

[35] P. M. Gresho and R. L. Sani. *Incompressible flow and the finite element method, Incompressible Flow & the Finite Element Method - Advection-Diffusion & Isothermal Laminar Flow.* John Wiley & Sons, June 1998.

[36] J. L Guermond, P. Minev, and J. Shen. An overview of projection methods for incompressible flows. *Computer methods in applied mechanics and engineering*, 195(44-47):6011–6045, 2006.

[37] M. D. Gunzberger. *Finite Element Methods for Viscous Incompressible Flows: A Guide to Theory, Practice, and Algorithms.* Academic Press Inc, 1989.

[38] L. Halpern and M. Schatzman. Artificial boundary conditions for incompressible viscous flows. *SIAM Journal on Mathematical Analysis*, 20(2):308–353, 1989.

[39] D. Hannasch and M. Neda. On the accuracy of the viscous form in simulations of incompressible flow problems. *Numerical Methods for Partial Differential Equations*, 28(2):523–541, 2012.

[40] J. G. Heywood, R. Rannacher, and S. Turek. Artificial boundaries and flux and pressure conditions for the incompressible Navier–Stokes equations. *International Journal for Numerical Methods in Fluids*, 22(5):325–352, 1996.

[41] T. J. R. Hughes and G. N. Wells. Conservation properties for the galerkin and stabilised forms of the advection–diffusion and incompressible Navier–Stokes equations. *Computer Methods in Applied Mechanics and Engineering*, 194(9–11):1141–1159, 2005.

[42] H. J. Kim, C. . Figueroa, T. J. R. Hughes, K. E. Jansen, and C. A. Taylor. Augmented Lagrangian method for constraining the shape of velocity profiles at outlet boundaries for three-dimensional finite element simulations of blood flow. *Computer Methods in Applied Mechanics and Engineering*, 198(45-46):3551–3566, 2009.

[43] A. P. Kuprat, S. Kabilan, J. P. Carson, R. A. Corley, and D. R. Einstein. A bidirectional coupling procedure applied to multiscale respiratory modeling. *Journal of Computational Physics*, 244:148–167, 2013.

[44] O. A. Ladyzhenskaya. *The mathematical theory of viscous incompressible flow*. Gordon and Breach, 1969.

[45] O. A. Ladyzhenskaya. Mathematical analysis of Navier–Stokes equations for incompressible liquids. *Annual Review of Fluid Mechanics*, 7(1):249–272, 1975.

[46] J. M. Leone and P. M. Gresho. Finite element simulations of steady, two-dimensional, viscous incompressible flow over a step. *Journal of Computational Physics*, 41(1):167–191, 1981.

[47] J. Leray. Étude de diverses équations intégrales non linéaires et de quelques problèmes que pose l'Hydrodynamique. *Journal de Mathématiques Pures et Appliquées*, 12:1–82, 1933.

[48] J. Leray. Essai sur les mouvements plans d'un fluide visqueux que limitent des parois. *Journal de Mathématiques Pures et Appliquées*, pages 331–418, 1934.

[49] S. Ley, D. Mayer, B. Brook, E. van Beek, C. Heussel, D. Rinck, R. Hose, K. Markstaller, and H.-U. Kauczor. Radiological imaging as the basis for a simulation software of ventilation in the tracheo-bronchial tree. *European radiology*, 12(9):2218–2228, 2002.

[50] A. C. Limache, P. J. Sánchez, L. D. Dalcín, and S. R. Idelsohn. Objectivity tests for Navier–Stokes simulations: The revealing of non-physical solutions produced by Laplace formulations. *Computer Methods in Applied Mechanics and Engineering*, 197(49):4180–4192, 2008.

[51] J.-L. Lions. *Quelques méthodes de résolution des problèmes aux limites non linéaires*. Dunod, 2002.

[52] J.-L. Lions and G. Prodi. Un théorème d'existence et d'unicité dans les équations de Navier–Stokes en dimension 2. *Comptes Rendus de l'Académie des Sciences de Paris Série I 248*, pages 3519–3521, 1959.

[53] D. Lombardi, T. Colin, A. Iollo, O. Saut, F. Bonichon, and J. Palussière. Some models for the prediction of tumor growth: general framework and applications to metastases in the lung. In *Computational Surgery and Dual Training*. Springer, 2014.

[54] M. Malvè, S. Chandra, J. L. López-Villalobos, E. A. Finol, A. Ginel, and M. Doblaré. CFD analysis of the human airways under impedance-based boundary conditions: application to healthy, diseased and stented trachea. *Computer Methods in Biomechanics and Biomedical Engineering*, pages 1–19, 2012.

[55] B. Maury. *The respiratory system in equations*, volume 7 of *MS&A. Modeling, Simulation and Applications*. Springer-Verlag Italia, Milan, 2013.

[56] B. Maury, N. Meunier, A. Soualah, and L. Vial. Outlet dissipative conditions for air flow in the bronchial tree. In *CEMRACS 2004 - Mathematics and applications to biology and medicine*, volume 14 of *ESAIM Proc.*, pages 201–212. EDP Sci., Les Ulis, 2005.

[57] V. Maz'ya and J. Rossmann. Point estimates for green's matrix to boundary value problems for second order elliptic systems in a polyhedral cone. *ZAMM - Journal of Applied Mathematics and Mechanics / Zeitschrift für Angewandte Mathematik und Mechanik*, 82(5):291–316, 2002.

[58] N. P. Moshkin and D. Yambangwai. On numerical solution of the incompressible Navier–Stokes equations with static or total pressure specified on boundaries. *Mathematical Problems in Engineering*, 2009, 2009.

[59] O. Pironneau. On the transport-diffusion algorithm and its applications to the Navier–Stokes equations. *Numerische Mathematik*, 38(3):309–332, 1982.

[60] O. Pironneau. Boundary conditions on the pressure for the Stokes and the Navier–Stokes equations. *Comptes Rendus de l'Académie des Sciences Série I Mathématiques*, 303(9):403–406, 1986.

[61] O. Pironneau. *Finite element methods for fluids*. Wiley, 1990.

[62] A. Porpora, P. Zunino, C. Vergara, and M. Piccinelli. Numerical treatment of boundary conditions to replace lateral branches in hemodynamics. *International Journal for Numerical Methods in Biomedical Engineering*, 28(12):1165–1183, 2012.

[63] A. Quarteroni and A. Valli. *Numerical approximation of partial differential equations*. Springer, 2nd edition, 2008.

[64] H.-G. Roos, M. Stynes, and L. Tobiska. *Robust numerical methods for singularly perturbed differential equations: convection-diffusion-reaction and flow problems*, volume 24 of *Springer Series in Computational Mathematics*. Springer-Verlag, Berlin, 2nd edition, 2008.

[65] R. L. Sani and P. M. Gresho. Résumé and remarks on the open boundary condition minisymposium. *International Journal for Numerical Methods in Fluids*, 18(10):983–1008, 1994.

[66] B. Sapoval. Smaller is better - but not too small: A physical scale for the design of the mammalian pulmonary acinus. *Proceedings of the National Academy of Sciences*, 99(16):10411–10416, 2002.

[67] A. Soualah-Alila. *Modélisation mathématique et numérique du poumon humain*. PhD thesis, Université Paris Sud, 2007.

[68] R. Temam. Une méthode d'approximation de la solution des équations de Navier–Stokes. *Bulletin de la Société Mathématique de France*, 96:115–152, 1968.

[69] R. Temam. Sur l'approximation de la solution des équations de Navier–Stokes par la méthode des pas fractionnaires (II). *Archive for Rational Mechanics and Analysis*, 33(5):377–385, 1969.

[70] R. Temam. *Navier-Stokes equations: theory and numerical analysis*, volume 2. American Mathematical Society, 2001.

[71] T. E. Tezduyar, S. Mittal, S. E. Ray, and R. Shih. Incompressible flow computations with stabilized bilinear and linear equal-order-interpolation velocity-pressure elements. *Computer Methods in Applied Mechanics and Engineering*, 95(2):221–242, 1992.

[72] T. E. Tezduyar and Y. Osawa. Finite element stabilization parameters computed from element matrices and vectors. *Computer Methods in Applied Mechanics and Engineering*, 190(3–4):411–430, 2000.

[73] J. Tu, K. Inthavong, and G. Ahmadi. *Computational fluid and particle dynamics in the human respiratory system*. Springer, 1 edition, 2012.

[74] C. Vergara. Nitsche's method for defective boundary value problems in incompressible fluid-dynamics. *Journal of Scientific Computing*, 46(1):100–123, 2011.

[75] I. E. Vignon-Clementel, C. A. Figueroa, K. E. Jansen, and C. A. Taylor. Outflow boundary conditions for three-dimensional finite element modeling of blood flow and pressure in arteries. *Computer Methods in Applied Mechanics and Engineering*, 195(29-32):3776–3796, 2006.

[76] W. A. Wall, L. Wiechert, A. Comerford, and S. Rausch. Towards a comprehensive computational model for the respiratory system. *International Journal for Numerical Methods in Biomedical Engineering*, 26(7):807–827, 2010.

[77] E. R. Weibel. *Morphometry of the Human Lung*. Springer-Verlag, 1963.